JPET Fast Forward. Published on January 12, 2007 as DOI: 10.1124/jpet.106.113019

JPET 113019

Title Page

Title: " Regulation of Oxidant-induced Intestinal Permeability by Metalloprotease-Dependent EGFR Signaling "

Forsyth CB, Banan A, Farhadi A, Fields JZ, Tang, Y, Shaikh M, Zhang LJ, Engen PA, Keshavarzian A.

Rush University Medical Center, Chicago, IL 60612

Department of Internal Medicine, Section of Gastroenterology (C.B.F, A.B., A.F., J.Z.F., Y.T., M.S., L.J.Z., P.A.E., A.K.)

Department of Pharmacology (A.B, A.K.)

Department of Physiology (A.K.)

Running Title Page

Running title: “Metalloprotease Regulation of Intestinal Permeability”

Corresponding Author:

Christopher B. Forsyth, Ph.D.

Assistant Professor of Medicine

Rush University Medical Center

Department of Internal Medicine, Section of Gastroenterology

1725 W. Harrison

Suite 206

Chicago, IL 60612

Tel. 312-942-9009

Fax. 312-942-5664

Email: christopher_b_forsyth@rush.edu

Text pages total- 48
Tables- 0
Figures- 15
References- 40
Abstract words= 247
Introduction words= 735
Discussion words= 1494

Recommended section assignment: Gastrointestinal, Hepatic, Pulmonary, and Renal

Abbreviations:

AKT-protein kinase B; DMSO-dimethyl sulfoxide; EGF-epidermal growth factor; EGFR-epidermal growth factor receptor; ERK1/2-extracellular signal regulated

kinases 1 and 2; GPCR-G protein-coupled receptor; HB-EGF- heparin binding epidermal growth factor; IBD-inflammatory bowel disease; IFN-γ-interferon-gamma; JNK1/2-jun kinases 1 and 2; MAPK-mitogen activated protein kinase; MLC-myosin light chain; MLCK- myosin light chain kinase; P38-38 kd protein (MAP kinase); PI3K-phosphatidylinositide 3'-OH kinase; SiRNA-short inhibitory ribonucleic acid; TACE-tumor necrosis factor-alpha converting enzyme; TAPI-tumor necrosis factor alpha protease inhibitor; TGF-α-transforming growth factor alpha; TJ-tight junction; TNF-α-tumor necrosis factor alpha.

Abstract

Background and Aims. Inflammatory bowel disease (IBD) affects more than one million Americans with more than 30,000 new cases diagnosed each year. IBD increases patient morbidity and susceptibility to colorectal cancer yet its etiology remains unknown. Current models identify two key determinants of IBD pathogenesis: (1) hyperpermeability of the gut epithelial barrier to bacterial products, and (2) an abnormal immune response to these products. Two factors appear critical for hyperpermeability: oxidant-induced stress and proinflammatory cytokines (e.g. TNF-α). The AIM of this study was to investigate the role of oxidant stress-mediated transactivation of the epidermal growth factor receptor (EGFR) in intestinal hyperpermeability. *Methods*. This study utilized the Caco-2 human colonic epithelial cell in vitro model of intestinal epithelium. Cells were grown on inserts for permeability and signaling studies and glass cover slips for microscopy studies. *Results*. We show oxidant-induced intestinal hyperpermeability can be blocked by specific inhibitors of the EGFR, tumor necrosis factor convertase (TACE) metalloprotease, TGF-α, and mitogen-activated protein kinases (MAPKs), especially ERK1/2. We also show that oxidant initiates these signaling events in part by causing translocation of TACE to cell-cell contact zones. *Conclusions.* In this study, our data identify a novel mechanism for oxidant-induced intestinal hyperpermeability relevant to IBD. We propose a new intestinal permeability model in which oxidant transactivates epidermal growth factor receptor (EGFR) signaling by activation of TACE and

cleavage of precursor TGF-α. These data could have a significant effect on our view of IBD pathogenesis and provide new therapeutic targets for IBD treatment.

Introduction

Inflammatory bowel disease (IBD) is a chronic intestinal inflammatory disorder that affects more than one million Americans with more than 30 thousand new cases diagnosed each year (Clayburgh et al., 2004; Farhadi, et al., 2003; Podolsky, 2002.) This disorder profoundly increases patient morbidity and decreases quality of life and increases patient susceptibility to colorectal cancer although its etiology remains unknown. Current models of disease pathogenesis identify as the two principal determinants of IBD pathogenesis: (1) increased permeability of the epithelial barrier of the intestinal mucosa which results in penetration of luminal bacterial products into the mucosa, and (2) an abnormal immune response to these products (Clayburgh et al., 2004; Farhadi et al., 2003). Regarding intestinal hyperpermeability in IBD, two factors are thought to play critical roles: oxidant-induced stress and proinflammatory cytokines, especially TNF-α and IFN-γ (Bruewer et al., 1998; Podolsky, 2002). The principal permeability pathway in IBD is the paracellular route, which is ultimately regulated by tight junctions (TJ) between the intestinal epithelial cells (IEC) that constitute the intestinal barrier (Clayburgh et al., 2004). Clearly, a better understanding of the mechanisms underlying oxidant-induced barrier disruption and intestinal hyperpermeability appears to be a key to understanding the pathogenesis of IBD. We therefore studied these mechanisms in the hope that it would suggest targets for novel interventions that interrupt pathogenic inflammatory cascades in IBD.

The study being reported herein, is part of our long-term goal of identifying mechanisms of oxidant-induced intestinal hyperpermeability using in vitro, animal, and clinical models of IBD (Banan et al., 2000a, 2000b; Keshavarzian et al., 1990). Using in vitro models of human intestinal epithelium this and other laboratories have identified key roles for specific intracellular signaling pathways mediating disruption of TJ permeability by oxidative stress. These pathways involve: signaling via the epidermal growth factor receptor (EGFR) (Banan et al., 2000a, 2000b, 2001a, 20001b), signaling via NF-kB activation (Banan et al., 2004), and signaling via specific protein kinase C (PKC) isoforms, which are either protective or injurious, depending on the PKC isoform (Banan et al., 2001b, 2005). Previous studies investigating a possible role for the EGFR in oxidant-induced intestinal hyperpermeability have determined that preincubation with epidermal growth factor (EGF) or transforming growth factor-alpha (TGF-α) prior to exposure to oxidant (H_2O_2) prevents oxidant-induced intestinal hyperpermeability (Banan et al., 2001b, 2002; Basuroy et al., 2006).

Recently, a new pathway for oxidant (H_2O_2) signaling through EGFR activation was identified. The pathway is 'metalloprotease dependent transactivation of EGFR signaling' (Fischer et al., 2004; Prenzel et al., 1999). In this model (See Fig. 15 below), metalloproteases, especially from the ADAM family of membrane-bound metalloproteases, become activated by a variety of signals and cleave EGFR precursor ligands attached to the cell surface. These solubilized ligands then bind to the EGFR and initiate EGFR-mediated signaling pathways (Schafer et al., 2004). Several studies have shown that oxidants (e.g.,

H_2O_2) are one of several stimuli capable of triggering signaling via ADAM-dependent transactivation of the EGFR (Schafer et al., 2004). The ADAM involved in greater than 80% of all cases is the tumor necrosis factor-α convertase: TACE (ADAM-17) (Black et al., 1997; Blobel, 2005). In the intestine, TACE levels are increased in the inflamed mucosa of patients with IBD and TACE inhibitors ameliorate colitis in animal models of IBD (Brynskov et al., 2002; Colon et al., 2001). We hypothesized that oxidant-induced metalloprotease-EGFR signaling could play a role in oxidant-induced increases in intestinal permeability characteristic of IBD.

In the present study we use an in vitro model of human intestinal epithelium to show that metalloprotease-EGFR signaling does play a key role regulating intestinal permeability in response to oxidant stress as well as baseline intestinal permeability. We identify TACE as the ADAM mediating EGFR transactivation through cleavage of TGF-α in response to oxidant stress. We also identify downstream EGFR-mediated mitogen-activated protein kinase (MAPK) signaling via ERK1/2 MAPKs to be necessary for oxidant-induced intestinal hyperpermeability. These data are the first demonstration of this EGFR transactivation mechanism regulating intestinal epithelial permeability. Also, oxidant stress is known to exist in IBD epithelium and TACE is required for TNF-α production so important in IBD pathogenesis. Therefore, stimulation of TACE activity by oxidant stress could clearly fuel IBD pathogenesis by stimulation of both TNF-α production and now we show through EGFR-mediated increased permeability resulting from TACE cleavage of TGF-α. This study could therefore

have significant implications towards new understanding of IBD pathogenesis in addition to providing new avenues for therapy of IBD.

Methods

Reagents. H_2O_2 (Sigma) was made fresh daily. TACE inhibitors used were TAPI-2 (N-(R)-[2-(Hydroxyaminocarbonyl)methyl]-4-methylpentanoyl-L-*t*-butyl-alanyl-L-alanine, 2-aminoethyl Amide, TNF-α Protease Inhibitor-2) (Chemicon, Temecula, CA), and GM6001, also known as Ilomastat or N-[(2R)-2-(hydroxamidocarbonylmethyl)-4-methylpentanoyl]-L-tryptophan methylamide, (Calbiochem, San Diego, CA). EGFR inhibitors used were: AG1478 (4-(3-Chloroanilino)-6,7-dimethoxyquinazoline) and GW2974 (N4-(1-Benzyl-1H-indazol-5-yl)-N6,N6-dimethyl-pyrido[3,4-d]pyrimidine-4,6-diamine) (Sigma); they show similar results in permeability and signaling studies. Kinase inhibitors (Calbiochem) were as follows**:** for ERK1/2 PD98059 (2-(2-Amino-3-methoxyphenyl)-4H-1-benzopyran-4-one) and U0126 (1,4-Diamino-2,3-dicyano-1,4-bis(o-aminophenylmercapto)butadiene ethanolate); for p38, SB203580 (4-(4-Fluorophenyl)-2-(4-methylsulfinylphenyl)-5-(4-pyridyl)-1H-imidazole); for JNK 1/2 inhibition, SP600125 (1,9-Pyrazoloanthrone Anthrapyrazolone); for PI3K inhibition, LY29004 (2-(4-morpholinyl)-8-phenyl-4H-1-benzopyran-4-one). Blocking antibodies (Abs) to EGFR (#LA1, Upstate, Temecula, CA) and EGFR ligands used were: Amphiregulin (R&D Systems, Minneapolis, MN), and TGF-α (R&D Systems); also the CRM197 HB-EGF blocker (diphtheria toxin)(Sigma, St. Louis, MO). We also used Ab to ZO-1 (Invitrogen, Carlsbad, CA) and a rabbit polyclonal anti-TACE Ab (Sigma). EGFR (Ab-1) and Phosphotyrosine Ab (4G10) and EGFR positive control were from Upstate. All other phospho and total MAPK

Abs and controls were from Cell Signaling Technology (CST) (Danvers, MA). These were comprised of (a) phospho-specific Abs including ERK1/2, p38, JNK1/2, AKT and total MAPK Abs (controls for loading) including ERK1/2, p38, JNK1/2, and AKT.

Cell culture. We used confluent human colonic epithelial Caco-2 cells (ATCC #CRL2101, C2BBe1, colorectal adenocarcinoma) or IEC-6 (rat, nontransformed intestinal epithelial, ATCC# CRL1592) between passages 15-25, grown on permeable culture inserts (Transwell, Corning, Corning, NY) for permeability and signaling studies, and grown on glass coverslips for microscope-based imaging studies. Cells were cultured at 37^{o}C/5% CO_2 in a humidified incubator in Delbecco's Modified Eagles Medium (DMEM)/10% Fetal Bovine Serum (FBS) media with 5 mM penicillin-streptomycin and 0.01 mg/ml human transferin.

Determination of integrity of the intestinal permeability barrier using monolayers of Caco-2 cells. Barrier permeability was determined using Caco-2 cells grown to confluence on 6.5 mm/0.2μm 24-well tissue culture plate inserts (Transwell, Corning) as we previously described (Banan et al. 2000a, 2000b). Permeability of insert Caco-2 monolayers was measured as apical to basolateral flux of the fluorescent marker fluorescein-5-(and-6)-sulfonic acid trisodium salt (FSA, 478 d) (Invitrogen) or FITC-dextran (fluorescein dextran 4 kd) (Sigma). This is an assay whose utility and validity has been shown and extensively used by others and ourselves and described (Banan et al., 2001a, 2001b; Sanders et al., 1995). Briefly, phenol red free, serum free DMEM (800 μl) was added into the lower (basolateral) chamber and DMEM (300 μl) with FSA (400nM) or FITC-dextran

(1.25 μM) into the upper (apical) chamber. At specific times, aliquots (50 μl) were transferred to opaque bottom, 96-well, fluorescence plates. Fluorescent signals were quantitated using a fluorescence plate reader and reported as "FSA or FITC-dextran Clearance" (nmol/cm^2/h). Excitation/emission spectra for FSA/FITC-dextran were: 485 nm/530 nm. Controls and a standard curve were done with each run. Inhibitors and blocking Abs were pre-incubated with cells for 1 h before adding H_2O_2.

Western blotting analysis. Western blotting (WB) was performed using the Biorad mini-Protean3 system as previously described (Forsyth et al., 2002). Cells were lysed with RIPA buffer containing protease and phosphatase inhibitor cocktails (Sigma) and 1 mg/ml PMSF (Phenylmethanesulfonyl fluoride) with 1% Nonidet P-40. Lysates were assessed for total protein (Biorad Laboratories, Hercules, CA) and 20 μg was loaded per lane of 4%/10% 1.0 mm Laemmli SDS PAGE gels. Protein was transferred to nitrocellulose and blocked with 5% bovine serum albumin (BSA) for 1 h at 4°C and then incubated at 4°C overnight with primary Ab. Blots were then washed, incubated with HRP-conjugated 2° Ab for 2 h at 4°C, washed, developed with ECL (GE Healthcare, Piscataway, NJ), exposed to film (Fuji, Tokyo, Japan), and scanned for densitometry analysis with NIH Image J software (Banan et al., 2005).

Isolation of RNA and RT-PCR. Isolation of total RNA was done using the RNEasy Kit (Qiagen, Valencia, CA). RNA was quantitated in a spectrometer. Reverse transcription of RNA to cDNA was carried out using the High Capacity cDNA RT Kit (Applied Biosystems, Foster, CA). Real time quantitative PCR was

then performed using the resulting cDNA with the Sybr Green PCR Master Mix (Applied Biosystems) and 35 cycles of 95°C-60°C-and 72°C (each 1 min) for PCR amplification. The reactions were performed in 96-well plates using an Applied Biosystems 7900HT Prism apparatus. Primers for RT-PCR used in the present study were: Beta actin (157bp): F:GCCAGGTCCAGACGCAGG; R:TGCTATCCAGGCTGTGCTA; TACE(154bp): :CTGTGGTGCAAAAGCAGAAA; R:TGCCAAATGCCTCATATTCA. Primers were designed with Oligoperfect software (Invitrogen) and purchased from Invitrogen. TACE data were normalized first to actin expression in the same sample and then normalized to the value of TACE expression in the "0 time" start cells to arrive at the fold expression value.

SiRNA inhibition studies. Smartpool short inhibitory RNA (siRNA) specific for human ADAM-17 (TACE) and control siRNA were purchased from Dharmacon (Dharmacon, Inc., Lafayette, CO). Caco-2 cells grown to 60% confluence in 6-well plates were transfected with 60 pmol/ml ADAM-17 siRNA or control siRNA using Lipofectamine (Invitrogen) and Optimem reduced serum media (Invitrogen) according to manufacturers instructions. At 7 days post treatment cells were assessed for expression of TACE protein using Western blotting. Cells with greater than 80% knockdown of TACE expression were then treated with H_2O_2 and assessed for ERK1/2 signaling and TACE expression by Western blot.

Microscopy. Microscopic images were obtained of Caco-2 cells grown to confluency plus 7 days on glass coverslips using an Axiovert 100 microscope and Axiovision software (Carl Zeiss Inc., Thornwood, NY). Two-dimensional

images (Figs. 10, 11, and 12) were obtained using an oil immersion 100x objective while images for Figs. 13 and 14 were obtained using an oil immersion 40x objective. Fig. 13 and Fig. 14 show images obtained by deconvolution of z-stack images (15 at 1 μm each). 3D reconstruction of deconvoluted z-stacks was performed using the Zeiss Axiovision software (Carl Zeiss Inc.). Immunfluorescent microscopic analysis of Caco-2 monolayers has been previously described by us in greater detail (Banan et al., 2001a, 2001b, 2004, 2005).

Statistical analysis. ANOVA to compare outcomes for 3 or more groups with $p \leq .05$ being considered significant. Data was analyzed using SPSS software for Windows (SPSS, Chicago, IL).

Results

EGFR-specific inhibitors, TACE-metalloprotease inhibitors, and inhibitors of MAPK ERK1/2 block H_2O_2-induced hyperpermeability across Caco-2 monolayers. Evidence summarized above supports oxidative stress as one of the principal causes of increased permeability in IBD that fuels the inflammatory response and tissue injury. Previous data from this and other laboratories suggests a role for pretreatment with EGFR ligands (EGF, TGF-α) in protection against IEC permeability caused by oxidative stress (Banan et al., 2000a, 2000b, 2001a, 2001b; Basuroy et al., 2006). In addition, recent discoveries have shown that metalloprotease-EGFR signaling mediates cellular response to H_2O_2 in other cell types (Fischer et al., 2004). Therefore, we sought to determine whether metalloprotease-EGFR signaling could be playing a role in increased permeability caused by oxidative stress in IBD. We used the in vitro Caco-2 insert monolayer model that has been well established by this and other laboratories as a reliable in vitro model of intestinal permeability (Banan et al., 2000a, 2000b; Basuroy et al., 2006). Permeability of monolayers was monitored by addition of the fluorescent dye fluorescein sulfonic acid (FSA,MW 478d) added at a concentration of 400 nM to the upper chamber and fluorescence of the lower chamber media (phenol-red free and serum-free DMEM) was assessed at 18 h and the data displayed in Fig. 1 as “FSA Clearance” (change in FSA at 490/530nM in the lower well) in nmol/cm^2/h (Banan et al., 2005; Sanders et al., 1995). All permeability data are means of triplicate wells from a representative

experiment of more than three such experiments. Using H_2O_2 as a model stimulus for oxidative stress, we subjected cells to 500 μM H_2O_2. This dose of H_2O_2 is consistent with the 200-500 μM range of H_2O_2 used by ourselves in previous studies and other investigators as a model stimulus of oxidative stress. (Fischer et al., 2004; Song et al., 2006). We have documented in previous studies that this dose does not significantly affect cell viability (Banan et al., 2000a, 2000b). This treatment caused a dramatic increase (~5 fold/h) in monolayer permeability without affecting cell viability (Fig. 1) and confirmed prior studies that oxidant stress increases Caco-2 permeability (Banan et al., 2001a, 2001b). The development of hyperpermeability was inhibited (-66%) by the EGFR-specific tyrosine kinase inhibitors AG1478 (500nM) (Fig. 1a, H_2O_2+EGFRi) and GW2901 (data not shown). It was inhibited to a somewhat greater extent (>70%) by the broad MMP-TACE inhibitor GM6001 (20 μM,) (Fig. 1a, MMPi) and the TACE-specific inhibitor TAPI-2 (10 μM)(Fig.1a, TACEi). The inhibition was significant ($p<.05$) compared to the H_2O_2+ DMSO control. These two inhibitors are known to markedly inhibit ADAM-17 (TACE) at the concentrations used (Mohler et al., 1994; Santiskulvong and Rozengurt, 2003). These data strongly support a TACE metalloprotease-EGFR transactivation mechanism, one requiring TACE cleavage of EGFR pro-ligands such as EGF, TGF-α, or HB-EGF. Also shown in Fig. 1a, AG1478 (control+EGFRi) as well as GM6001 (control+MMPi) and TAPI-2 (control+TACEi) also caused small but significant ($p<.05$) increase in permeability relative to control wells treated only with media + vehicle (control+DMSO). These data support a role for TACE-

EGFR signaling in regulation of baseline intestinal epithelial permeability as well. Taken together these data strongly support a role for TACE-EGFR signaling in regulation of both the baseline permeability function as well as in response to the IBD relevant oxidative stress model stimulus H_2O_2.

In light of these data, we next sought to determine whether the EGFR and TACE inhibitors could protect against oxidant-induced changes in the key tight junction protein ZO-1. We and others have previously shown that another Caco-2 model system can be used to investigate mechanisms of H_2O_2-induced changes in IEC permeability (Banan et al., 2005; Basuroy et al., 2006). Cells grown to confluence on glass coverslips can be treated under the same experimental conditions, fixed, and stained for the TJ protein ZO-1 (Fig. 1b i-iv). Increased displacement ('zig-zag' pattern) of ZO-1 in this system correlates well with oxidant induced increased monolayer permeability (Banan et al., 2005, Basuroy et al., 2006). Immunofluorescence microscopy clearly shows that the dramatic displacement of ZO-1 caused by H_2O_2 (Fig. 1b-ii) is prevented by pretreatment of cells with the EGFR kinase-specific inhibitor AG1478 (Fig. 1b-iii) or the TACE-specific inhibitor TAPI-2 (Fig.1b-iv). These data further support a requirement for EGFR and TACE-mediated signaling in oxidant-induced increased barrier permeability shown in Fig. 1a.

These above data support a requirement for EGFR signaling in oxidant-induced intestinal epithelial permeability. Therefore, we next sought to determine what key downstream EGFR signaling pathways might be mediating the increase in permeability.

Key signaling pathways activated by EGFR signaling in other cell types include MAPK and AKT signaling (Fischer et al., 2004; Schafer et al., 2004). We thus determined the effect on H_2O_2-induced hyperpermeability of inhibitors of three principal MAPK pathways: ERK1/2, JNK1/2, and p38 as well as the effect of inhibition of PI3K activation of AKT (Fig.1c). Of the inhibitors tested, Fig. 1c shows only the ERK1/2 inhibitors PD98059 (20 μM) and U0126 (20 μM) (not shown) inhibited oxidant-induced permeability in a manner as great as the EGFR or MMP inhibitors in Fig. 1a. These data suggest that ERK1/2 activation is one major downstream signaling mechanism for EGFR-mediated hyperpermeability in response to H_2O_2 stimulation. Finally, we sought to validate the FSA permeability data with another marker of IEC permeability. We used the well validated 4kd FITC-dextran marker (1.25 μM) added to the apical surface of transwells and assessed movement to the lower chamber over 18h as for FSA above (Fig. 1d). As for FSA, oxidant-induced permeability to 4 kd FITC-dextran was substantially increased over 18h and this increase could be virtually eliminated by pretreatment with the EGFR, metalloprotease, and ERK inhibitors.

EGFR-specific inhibitors and TACE-metalloprotease inhibitors block H_2O_2-induced EGFR and ERK1/2 phosphorylation in Caco-2 monolayers. To further elucidate TACE-EGFR signaling mechanisms, we performed phosphoprotein analysis of cell lysates from cells stimulated with H_2O_2 with or without inhibitors of EGFR, TACE or ERK1/2 (Figs. 2a and 2b). From Fig. 2a it is clear that inhibitors of EGFR (AG1478) and TACE (TAPI-2) substantially block H_2O_2-stimulated EGFR phosphorylation (>90%). The effect of the TACE inhibitor supports a

TACE-dependent transactivation mechanism involving cleavage of EGFR pro-ligands as a requirement for H_2O_2-induced EGFR phosphorylation. In addition, the ERK1/2 inhibitor (PD98059) had no significant effect on EGFR phosphorylation. This suggests EGFR phosphorylation is upstream of ERK1/2 activation.

Besides EGFR phosphorylation, the parameter most often used to assess EGFR activation/signaling is phosphorylation (activation) of the MAPKs ERK1 and ERK 2 (ERK1/2) (Prenzel et al., 1999; Schafer et al., 2004). Fig. 2b shows that both EGFR and TACE inhibitors reduce ERK1/2 activation to below control levels. As expected, the MEK-1 inhibitor PD98059 also eliminates ERK1/2 activation. Taken together, the phosphoprotein signaling data from Fig. 2a and Fig 2b support a metalloprotease-dependent transactivation model in which oxidant stress-induced EGFR phosphorylation is upstream of ERK1/2 activation and that the activity of TACE or another ADAM metalloprotease (inhibited by TAPI-2) is required for oxidant-induced EGFR phosphorylation. We also wished to establish that H_2O_2-induced signaling via EGFR-metalloprotease activation could be demonstrated in other IEC cell lines and not only in Caco-2 cells. To do this we utilized IEC-6 cells, a non-transformed rat cell line widely used in intestinal epithelial models. Confluent cells were treated with H_2O_2 ± an EGFR inhibitor (AG1478) or TACE inhibitor (TAPI-2) and assessed for ERK1/2 activation with phosphospecific Abs as in Fig. 2b. As with the Caco-2 cells, oxidant induced a greater than five-fold increase in ERK1/2 phosphorylation that was inhibited by both the EGFR inhibitor (75%) and the TACE inhibitor (82%).

These data further support the EGFR-metalloprotease model of H_2O_2-induced signaling in IEC and that it is also true for other intestinal epithelial cells.

SiRNA studies identify TACE as the principal metalloprotease mediating H_2O_2-induced EGFR signaling in Caco-2. Because chemical inhibition of metalloproteases is not gene specific, we next sought to establish whether TACE or another metalloprotease was mediating H_2O_2-induced EGFR signaling in IEC using gene specific knockdown of TACE with short inhibitory RNA (siRNA) (Fig. 4). We used Smartpool siRNA from Dharmacon specific for human ADAM-17 (TACE) and used by another group to successfully knockdown TACE (Fischer et al., 2005) and transfected the siRNA (60 pmol/ml) under optimized conditions into Caco-2 cells grown to 60% confluency. After 7 days cells were treated with H_2O_2 and the response to oxidant was assessed by ERK1/2 phosphorylation. Blots were also stripped and reprobed with Ab to TACE to assess expression of TACE 110kd and 90kd forms. The data shown in Fig. 4 reveal that in cells in which TACE protein expression was knocked down by 84% (lane 3, TACE siRNA) compared to the control siRNA treated cells (lane 4) the H_2O_2-induced ERK1/2 activation was also reduced by 85% ($p<.05$) compared to the control siRNA-treated cells. Our previous data above showed that H_2O_2-induced ERK1/2 activation in Caco-2 is EGFR and metalloprotease dependent and that ERK1/2 activation is required for H_2O_2-induced hyperpermeability. Therefore, while these data do not rule out participation of other metalloproteases, they do demonstrate in a gene-specific manner that TACE is the principal ADAM metalloprotease

mediating H_2O_2-induced EGFR-ERK1/2 signaling and therefore increased permeability by this mechanism in Caco-2 cells.

TACE protein is abundantly expressed by Caco-2 cells and EGFR and TACE inhibitors do not act by inhibiting TACE protein expression. Because the above data point to a role for TACE in H_2O_2-induced signaling and permeability, we wished to determine whether sufficient quantities of TACE were expressed by Caco-2 cells and how EGFR, TACE, and ERK1/2 inhibitors affected TACE protein expression. TACE protein was assessed using Western blotting of cell lysates with polyclonal antibody to the TACE cytoplasmic domain (Fig. 5). Studies of other cell types including Caco-2 cells have shown that production of TACE is relatively constant and that TACE exists in the cell as an intracellular, 110 kd, inactive zymogen, “pro-TACE” form and an activated 90 kd form predominantly found on the cell surface or near the cell surface in intracellular vesicles (Schlondorff et al., 2000; Soond et al., 2005). The 110 kd pro-TACE appears to be associated with the cytoskeleton in a perinuclear location (Soond et al., 2005). The data from Caco-2 cells in Fig. 3 is in lanes 2-6. Lane 1 “+Con” contains a TACE positive control cell lysate (Chemicon). The 15 min timepoint chosen was the same as that for the EGFR and ERK1/2 signaling data for comparison. No significant differences in TACE protein expression from these data were seen with the EGFR and TACE inhibitors in 18h lysates (not shown). Clearly, Caco-2 cells even at rest express abundant TACE in both the Pro-110 kd as well as the activated 90 kd forms (lane 2). Also, treatment with H_2O_2 results in only a slight increase (but not statistically significant) in both the 110 kd and 90

kd forms of TACE (lane 3). However, in the presence of H_2O_2, treatment with the EGFR inhibitor (lane 4), TACE inhibitor (lane 5) or the ERK1/2 inhibitor (lane 6) did not significantly alter the amount of Pro- or activated TACE to an extent that would account for complete blocking of EGFR or ERK1/2 phosphorylation as seen in Fig.2. In fact the amount of active 90 kd TACE is relatively constant in lanes 2-6 with no statistical difference detected. The blot was stripped and reprobed with Ab to actin as a protein loading control. Taken together, these data show that strong expression of TACE protein by Caco-2 in our system is consistent with other data above pointing to a role for TACE in oxidant-induced EGFR-mediated signaling and permeability changes. However, activation of TACE-mediated EGFR signaling does not appear to be related to changes in the active form of TACE protein.

While no changes in TACE protein expression were seen either at 15min or 18h, we wished to assess whether changes in TACE gene expression (mRNA) could account for increased TACE signaling required for H_2O_2-induced permeability (Fig. 6). We also wished to determine whether gene expression (mRNA) of TACE was altered in cells after H_2O_2 treatment for 18 h +/- EGFR inhibitor. In addition, cells were treated with epidermal growth factor (EGF) which we have shown in previous studies to prevent H_2O_2-induced permeability in Caco-2 inserts (Banan et al., 2000a, 2000b). In Fig. 6 data from quantitative real time RT-PCR for TACE is normalized in each lane to actin expression and that ratio is expressed as a fold expression of the start control (histogram). Treatment with H_2O_2 alone resulted in reduced TACE expression while treatment with the

EGFR inhibitor resulted in increased TACE expression. Interestingly, treatment with EGF also resulted in downregulation of TACE expression. These data suggest a negative feedback mechanism that regulates TACE expression when EGFR signaling is stimulated by oxidants or EGF. Clearly, however, these data do not support increased TACE gene expression as the probable mechanism for oxidant-induced hyperpermeability through EGFR-TACE signaling.

Permeability and signaling data support TGF-α as the EGFR ligand mediating increased permeability in response to oxidant. A key element in metalloprotease-EGFR transactivation is the EGFR proligand cleaved on the surface of the cell by TACE. To identify this ligand, we assessed the effects of blocking proteins to the EGFR and EGFR ligands on hyperpermeability induced by H_2O_2 (Fig. 7). Blocking antibodies to amphiregulin had no effect at several concentrations (not shown). The blocking protein for HB-EGF (CRM197, 10 μg/ml, a diphtheria toxin) had a dramatic effect on resting cells (bar 3), increasing permeability to that of H_2O_2 treated cells, but had little effect at blocking H_2O_2-induced permeability (bar 7). In contrast, blocking Ab to TGF-α (10 μg/ml) had little effect on resting permeability (bar 4) but blocked H_2O_2 induced hyperpermeability by 96% (bar 8). Cells treated with blocking Ab to the EGFR caused some leakiness in control cells and blocked H_2O_2 induced hyperpermeability by 80%. These data support a role for TGF-α as the oxidant-stimulated proligand cleaved by TACE that subsequently binds to the EGFR to induce ERK1/2 and other signals required for increased permeability. Surprisingly, because blocking HB-EGF and the EGFR caused increased

baseline permeability, these data also suggest a role for the EGFR in the mediation of baseline permeability.

To further evaluate TGF-α and HB-EGF signaling after oxidant stimulation, we carried out phosphoprotein analysis of cell lysates to assess EGFR phosphorylation (Fig. 8) and ERK1/2 activation (Fig. 9) in the presence of the above EGFR, TGF-α, and HB-EGF inhibitors when cells were at rest or stimulated with H_2O_2. The EGFR activation data (Fig. 8) agree closely with the ERK1/2 signaling data (Fig.9). Fig. 8, lane 3 shows cells that were treated with the EGFR inhibitor AG1478 –all baseline EGFR phosphorylation was eliminated. The solid bars indicate treatment with H_2O_2. H_2O_2 greatly stimulated EGFR phosphorylation (Lane 4). Pretreatment with EGFR kinase inhibitor (lane 5) and TACE inhibitor (lane 6) again reduced EGFR tyrosine phosphorylation to below control (baseline) levels seen in lane 2 in spite of H_2O_2 stimulation. Thus, as in Fig. 2a above, virtually all H_2O_2-stimulated EGFR phosphorylation was found to be metalloprotease-dependent. Next, specific blocking proteins or Abs to the EGFR or EGFR ligands amphiregulin, HB-EGF and TGF-α were tested for their effect on cell signaling at concentrations equal to those used in the Fig. 7 permeability studies. Blocking Ab to the EGFR significantly inhibited (to below control levels) EGFR phosphorylation stimulated by H_2O_2 (Lane 7). Most important, treatment with blocking Ab to TGF-α eliminated EGFR phosphorylation to a level comparable to the effects of EGFR kinase and TACE inhibitors, while blocking protein to HB-EGF inhibited by only 40%. We next assessed ERK1/2 phosphorylation in the same cell lysates (Fig. 9). Lane 2

shows that virtually all ERK1/2 activation is due to EGFR signaling and is eliminated with EGFR kinase inhibitor treatment, even in control cells (baseline). H_2O_2 dramatically stimulated ERK1/2 activation (five-fold) (lane 3), and the EGFR kinase (lane 4) and TACE inhibitors (lane 5) blocked activation of downstream signaling, in this case ERK1/2, to below baseline control values. The blocking Ab to the EGFR (anti-ErbB1) also significantly (-88 %) inhibited oxidant-induced ERK1/2 activation, but not to the extent (≥ 95 %) of the blocking TGF-α antibody. Finally, blocking protein to HB-EGF inhibited H_2O_2 induced ERK1/2 activation, but only by 30%. Blocking Ab to amphiregulin had no effect on EGFR or ERK1/2 phosphorylation at several concentrations (not shown). Taken together, these permeability and phosphoprotein signaling data strongly support a metalloprotease-dependent EGFR transactivation mechanism regulating permeability of this in vitro model in response to oxidant stress. In addition the data support a model in which TGF-α is the pro-ligand cleaved by TACE to initiate the EGFR-ERK1/2 signaling required for the increase in permeability.

The EGFR as well as the EGFR proligands TGF-α and HB-EGF are primarily localized to peripheral cell-cell junctions. We next sought to use immunofluorescence microscopy to identify the cellular locations of the EGFR and EGFR proligands TGF-α and HB-EGF. Fig. 10 shows the results from staining unstimulated Caco-2 monolayers on coverslips with primary Ab to the EGFR (ErbB1) followed with FITC secondary Ab (green) as well as Ab to TACE followed by Texas Red secondary Ab. Clearly, the EGFR location is concentrated at the cell periphery in areas of cell-cell adhesion (arrows). No differences were

seen after treatment with H_2O_2 (not shown). Figures 11a and 11b show representative images resulting from Caco-2 on coverslips with primary Ab to either HB-EGF (Fig. 11a) or TGF-α (Fig. 11b) followed by FITC secondary Ab. Again, in both cases the EGFR proligands are also primarily localized to cell-cell contact zones, which also did not change with oxidant stimulation (not shown).

We next used immunofluorescent microscopy to identify the location of TACE before and after stimulation with oxidant (Figs. 12-14). To do this, we treated cells with Ab to: 1) the intracellular domain of TACE (+Texas Red 2°Ab), and 2) the tight junction protein ZO-1 (+FITC 2°Ab) either as media treated control (upper panel, 12a-c) cells or cells treated with H_2O_2 (lower panel, 12d-f). These images are representative of multiple experiments and images and clearly show several key points. First, note the characteristic deformation of ZO-1 staining in the H_2O_2 treated (lower) panel as seen in Fig.1 that is consistent with increased permeability. The next point is that TACE staining in unstimulated cells is characteristically without pattern and distributed diffusely within each cell as viewed in 2D (arrows). However, in oxidant stimulated cells TACE staining consistently exhibits a strong distribution to the cell periphery and forms characteristic 'ring-like' structures (arrows). Thus, stimulation with oxidant appears to result in dramatic TACE translocation to the cell-cell contact zones where the EGFR, TGF-α, and HB-EGF are already located. The translocation of TACE to co-localize with ZO-1 is shown in the x-z views compiled from deconvoluted z-stacks in Fig. 13. In the Fig. 13 x-z and y-z projections note the large distribution of TACE (red) below the plane of ZO-1 (green) in Control cells

(unstimulated), while TACE can clearly be seen to colocalize with ZO-1 in the H_2O_2-stimulated cells. This redistribution of TACE to co-localize with ZO-1 is most clear in the 3-D reconstructions seen in Fig. 14. In Fig 14A and 14B the TACE (red) pool is clearly located beneath ZO-1 (green) in a virtual bilayer arrangement. Dramatically, in the oxidant stimulated cells, TACE translocates to colocalize and intersperse with ZO-1 and the lower pool of TACE disappears (Fig. 14C, Fig.14D). In the unstimulated cells, TACE (red) exists predominantly in a pool beneath ZO-1 (green) that is perinuclear as reported by others in different cell types (Soond et al., 2005). Staining for nuclei with DAPI has been left out of these figures because it obscured the view of TACE staining, however the perinuclear (lower) pool of TACE is still clear in the 3D views in Figs.14A and 14B. The lower TACE pool is especially clear in Figs. 14A (orthogonal, from below) and this clearly becomes intercalated with ZO-1 in Fig. 14C. Taken together, these series of fluorescence microscopic images in Figs 12-14 clearly demonstrate movement of TACE to colocalize with ZO-1 in oxidant stimulated cells consistent with the proposed role for TACE in regulating TJ permeability in IEC.

Discussion

TNF-α and oxidants are widely acknowledged as key proinflammatory factors involved in tissue injury in both ulcerative colitis and Crohn's disease (Farhadi et al., 2003; Podolsky, 2002). Indeed, anti-TNF-α (Zeissig et al., 2002) or antioxidant (Keshavarzian et al., 1992) therapies have been shown to be effective in the treatment of IBD. One of the mechanisms underlying the deleterious effects of oxidants and TNF-α in IBD is probably increased intestinal permeability (Bruewer et al., 2003; Clayburgh et al., 2004). However, the mechanisms of oxidant and TNF-α induced intestinal hyperpermeability in IBD are not fully understood. It is known that TACE is the metalloprotease required for TNF-α cleavage and biological activity (Black et al., 1997). Both TACE and TNF-α are upregulated in active IBD as well as in normal-appearing mucosa of IBD patients (Brynskov et al., 2002; Zeissig et al., 2004). TNF-α is also known to stimulate TACE expression in a kind of vicious circle (Black et al., 1997). Our study now provides the novel finding that oxidant-induced barrier hyperpermeability is partly dependent on TACE metalloprotease-mediated transactivation of EGFR signaling. This study provides compelling data to support a new model (oxidant-induced metalloprotease dependent EGFR transactivation) that could identify a new relationship between oxidants and TNF-α in inducing intestinal hyperpermeability and tissue injury in IBD. The key points of this model are summarized in Fig. 15. The model begins with oxidant stress (#1) resulting in activation of the metalloprotease TACE (#2). Activated TACE then cleaves membrane TGF-α to a soluble form (#3) that binds to the EGFR.

EGFR activation then results in downstream MAPK/ERK1/2 activation (#4). ERK1/2 signaling (#5) then results in increased intestinal permeability (#6) by pathways that have yet to be identified.

Metalloprotease-EGFR signaling has been demonstrated in IEC in response to Substance-P (Koon et al., 2004), and *C. difficile* toxin (Na et al., 2005) as a regulator of cell proliferation. Previous studies from this and other laboratories have shown a role for the EGFR in regulation of intestinal permeability in response to oxidative stress (Banan et al., 2000a, 2001a; Basuroy et al., 2006). To our knowledge, however, ours is the first demonstration of metalloprotease-EGFR transactivation signaling in the regulation of intestinal barrier function by any stimulus, and in this case in response to oxidative stress.

Several of our results strongly support TACE as the primary metalloprotease involved. First is potent inhibition of oxidant-induced intestinal hyperpermeability by GM6001 as well as by the TACE-specific inhibitor TAPI-2. TACE is not an MMP but is instead a member of the ADAM family of membrane metalloproteases. While also capable of inhibiting MMP type metalloproteases, GM6001 has been shown by others to inhibit TACE but not necessarily other ADAM metalloproteases (Santiskulvong and Rozengurt, 2003). In contrast TAPI-2 was originally identified by its ability to inhibit TACE but not MMPs, however its specificity against other ADAM metalloproteases in the TACE family is not well defined (Mohler et al., 1994). Second, both the EGFR and TACE inhibitors also block oxidant-induced displacement in ZO-1 staining that are characteristic of increased permeability (Banan et al., 2001a; Basuroy et al., 2006). Third, RT-

PCR and Western-blotting data show that Caco-2 cells in our model express abundant TACE, including the key 90 kd activated form (Black et al., 1997). Fourth, gene-specific siRNA knockdown studies of TACE reveal that TACE is the predominant metalloprotease mediating H_2O_2-induced ERK1/2 activation required for increased permeability in our model. Fifth and finally, significantly, our images also show that with oxidant stimulation TACE is translocated to cell-cell junction areas and colocalizes with ZO-1 in proximity with the proposed ligand/receptor in this case: TGF-α/EGFR. These translocation images support a model proposed by others for translocation of TACE with specific proligand substrates as a key regulatory mechanism of TACE specificity (Werb and Yibing, 1998). Our TGF-α permeability and signaling blocking data clearly support that TGF-α is the principal EGFR proligand cleaved by TACE upon H_2O_2 stimulation and these data are further supported by the dramatic peripheral co-localization of TACE-TGF-α in oxidant stimulated cells. This is consistent with TACE being the major sheddase for TGF-α cleavage in EGFR transactivation in other cell types (Blobel, 2005).

Our data show the mechanism for increased permeability due to H_2O_2 transactivation of EGFR signaling is mediated in part by MAPK signaling, specifically ERK1/2. Thus another concept that emerges form this study is that ERK1/2 activation appears to be one critical pathway mediating intestinal hyperpermeability in response to oxidants through TACE-EGFR signaling. This is supported by the comparative permeability and signaling data since only the EGFR, TACE, and ERK1/2 inhibitors showed similar protection against increased

permeability and these three inhibitors exhibited the most significant inhibition of both EGFR and ERK1/2 activation by oxidants. This data agrees with that of others showing tyrosine kinase and Src inhibitors block H_2O_2-induced permeability in Caco-2 monolayers (Basuroy et al., 2003). This result also agrees with data from others showing that both TGF-α induced hyperpermeability in MDCK cells (Chen et al., 2000), and H_2O_2-induced endothelial hyperpermeability (Fischer et al., 2005) can be blocked with the same ERK1/2 inhibitor. However, these data seem to differ from other studies showing ERK1/2 activation is required for EGF protection of Caco-2 monolayers from oxidant stress-induced hyperpermeability. The reason for this difference is not clear. One possibility is that the study referred to used very low concentrations of H_2O_2 (20μM) which do not result in ERK1/2 activation in their data or in our laboratory. Therefore the mechanism and role of ERK1/2 may be different. The concentration of H_2O_2 used in the present study is consistent with the 200-500μM concentration utilized by other investigators in the initial discovery of oxidant-induced EGFR transactivation (Prenzel et al., 1999) as well as more recent intestinal epithelial cell studies by others (Song et al., 2006). We have stated here and in previous studies this concentration does not affect cell viability (Banan et al., 2000a, 2000b).

Another key difference is the point we refer to as the “EGF-EGFR paradox”. The paradox is as follows: Pre-incubation with EGFR ligands EGF or TGF-α protects against oxidant induced permeability. However, paradoxically, EGFR signaling appears to be required for oxidant-induced permeability. The

mechanism for this at present is unknown, but has precedent in many of the preconditioning models in cell biology in which preconditioning with a stimulus 'protects' against subsequent challenge with that stimulus (e.g. heat shock, hypoxia). In fact, ERK1/2 have been shown to be important in oxidant preconditioning in other cell types (Hung et al., 2003). While our own studies have shown previously that PLC-gamma (Banan et al., 2001a) and PKC-β1 (Banan et al., 2002) are also critical for this EGF preconditioning protection, the complete mechanism for this paradox remains to be identified in future studies but appears to also require ERK1/2 signaling (Basuroy et al., 2006). Taken together it is clear that EGFR signaling as well as ERK1/2 signaling play critical roles in oxidant induced intestinal permeability and protection.

Our data showing that ERK inhibitors block oxidant-induced hyperpermeability agrees with studies with MDCK and endothelial cells. Therefore, key downstream targets of ERK appear to be critical in the regulation of paracellular permeability in many cell types. One possible candidate suggested in other studies is Myosin light chain kinase (MLCK) (Clayburgh et al., 2004). ERK1/2 directly phosphorylates MLCK (Nguyen et al., 1999), and MLCK activation of myosin light chain (MLC) is one key mechanism regulating intestinal permeability and may play a role in IBD (Clayburgh et al., 2004). In addition, ERK1/2 can be immunoprecipitated with the TJ protein occludin in oxidant treated IEC (Basuroy et al., 2006), suggesting phosphorylation of occludin by ERK1/2 as another mechanism for ERK1/2 regulation of TJ permeability. Finally, ERK1/2 have been shown to regulate TACE activation and phosphorylate TACE

directly (Soond et al., 2005). Further studies will be needed to identify the specific role(s) for ERK1/2 in TACE/EGFR regulation of intestinal permeability.

In summary, we propose a new model in which metalloprotease-dependent EGFR transactivation in response to oxidant stress is one mechanism for intestinal hyperpermeability and tissue injury in IBD. In this model the metalloprotease TACE plays a key role by cleavage of EGFR ligands and TNF-α. Indeed, metalloprotease inhibitors of TACE eliminate inflammation in animal models of IBD (Colon et al., 2001). Our permeability data with the CRM197 specific blocking protein for HB-EGF and our microscopy data showing it localized to cell-cell junction zones support a model in which HB-EGF signaling regulates baseline barrier integrity. This could occur possibly via juxtacrine interaction by HB-EGF proligands with EGFR on neighboring cells which is known to inhibit mitosis (Singh et al., 2004).

Thus, our findings could have far-reaching implications for a better understanding of IBD pathogenesis using a new model of intestinal hyperpermeability. These data also identify potential targets for developing new therapies for IBD such as specific inhibitors of TACE-EGFR initiated signaling and ERK1/2 inhibitors. Further in vivo animal studies are currently underway in our laboratory to determine whether modulation of the metalloprotease-dependent EGFR transactivation pathway can be successfully and safely targeted in IBD therapy.

References

Banan A, Zhang Y, Losurdo J, and Keshavarzian A. 2000a. Carbonylation and disassembly of the F-actin cytoskeleton in oxidant-induced barrier dysfunction and its prevention by epidermal growth factor and transforming growth factor-α in a human intestinal cell line. Gut. 46: 830-837.

Banan A, Choudhary S, Zhang Y, and Keshavarzian A. 2000b. Role of the microtubule cytoskeleton in protection by epidermal growth factor and transforming growth factor-α against oxidant-induced barrier disruption in a human colonic cell line. Free Radical Biol Med. 28:727-738.

Banan A, Fields JZ, Zhang Y, and Keshavarzian A. 2001a. Phospholipase C-gamma inhibition prevents EGF protection of intestinal cytoskeleton and barrier against oxidants. Am J Physiol Gastrointest Liver Physiol. 281:G412-G423.

Banan A, Zhang Y, Fields JZ, and Keshavarzian A. 2001b. Key role of PKC and calcium homeostasis in epidermal growth factor-induced protection of the microtubule cytoskeleton and intestinal barrier against oxidant injury. Am. J. Physiology 2001b. 280:G828-G843.

Banan A, Fields JZ, Farhadi A, Talmadge DA, Zhang Y, and Keshavarzian A. 2002. The beta 1 isoform of protein kinase C mediates the protective effects of epidermal growth factor on the dynamic assembly of F-actin cytoskeleton and

normalization of calcium homeostasis in human colonic cells. J Pharmacol Exp Ther. 301:852-866.

Banan A, Zhang LJ, Shaikh M, Fields JZ, Farhadi A, and Keshavarzian A. 2004. Novel effect of NF-kB activation: carbonylation and nitration injury to cytoskeleton and disruption of monolayer in intestinal epithelium. Am J Physiol Cell Physiol. 287:C1139-C1151.

Banan A, Zhang LJ, Shaikh M, Fields JZ, Choudhary S, Forsyth, CB, Farhadi A, and Keshavarzian A. 2005. Theta isoform of protein kinase C alters barrier function in intestinal epithelium through modulation of distinct claudin isotypes: a novel mechanism for regulation of permeability J Pharm Exper Therap. 313:962-982.

Basuroy S, Seth P, Kuppuswamy D, Balasubramanian S, Ray RM, and Rao RK. 2003. Expression of kinase-inactive c-Src delays oxidative stress-induced disassembly and accelerates calcium-mediated reassembly of tight junctions in the Caco-2 cell monlayer. J Biol Chem. 278:11916-11924.

Basuroy S, Seth A, Elias B, Anjaparavanda P, Naren A, and Rao R. 2006. MAP kinase interacts with occludin and mediates EGF-induced prevention of tight junction disruption by hydrogen peroxide. Biochem J. 393:69-77.

Black RA, Rauch CT,Kozlosky CJ, Peschon JJ, Slack JL, Wolfson MF, Castner BJ, Stocking KL, Reddy P, Srinivasan S, Nelson N, Boiani N, Schooley KA, Gerhart M, Davis R, Fitzner JN, Johnson RS, Paxton RJ, March CJ, and Cerritti DP. 1997. A metalloproteinase disintegrin that releases tumor-necrosis factor-alpha from cells. Nature. 385:729-733.

Blobel CP. 2005. ADAMs: key components in EGFR signaling and development. Nat Rev Mol Cell Biol. 6:32-43.

Bruewer M, Luegering A, Kucharzik T, Parkos CA, Madara JL, Hopkins AM, and Nusrat A. 2003. Proinflammatory cytokines disrupt epithelial barrier function by apoptosis-independent mechanisms. J Immunol. 171:6164-6172.

Brynskov J, Foegh P, Pederson G, Ellervik C, Kirkegaard T, Bingham A, and Saermark T. 2002. Tumor necrosis factor converting enzyme (TACE) activity in the colonic mucosa of patients with inflammatory bowel disease. Gut. 51:37-43.

Chen Y, Lu Q, Schneeberger EE, and Goodenough DA. 2000. Restoration of tight junction structure and barrier function by down-regulation of the mitogen-activated protein kinase pathway in Ras-transformed Madin-Darby canine kidney cells. Mol Biol Cell. 11:849-862.

Clayburgh DR, Shen L, and Turner JR. 2004. A porous defense: the leaky epithelial barrier in intestinal disease. Lab Invest. 84:282-291.

Colon AM, Menchen LA, Hurtado O, De Cristobal J, Lizasoain I, Leza JC, Lorenzo P, and Moro MA. 2001. Implication of TNF-alpha convertase (TACE/ADAM17) in inducible nitric oxide synthase expression and inflammation in an experimental model of colitis. Cytokine. 16:220-226.

Farhadi A, Banan A, Fields J, and Keshavarzian A. 2003. Intestinal barrier: an interface between health and disease. J Gastroenterol Hepatol. 18:479-487.

Fischer OM, Hart S, Gschwind A, Prenzel N, and Ullrich A. 2004. Oxidative and osmotic stress signaling in tumor cells is mediated by ADAM proteases and heparin-binding epidermal growth factor. Mol Cell Biol. 24:5172-5183.

Fischer S, Wiesnet M, Renz D, Schaper W. 2005. H_2O_2 induces paracellular permeability of porcine brain-derived microvascular endothelial cells by activation of the p44/42 MAP kinase pathway. Eur J Cell Biol. 84:687-697.

Forsyth CB, Pulai J, and Loeser RF. 2002. Fibronectin fragments and blocking antibodies to alpha2beta1 and alpha5beta1 integrins stimulate mitogen-activated protein kinase signaling and increase collagenase 3 (matrix metalloproteinase 13) production by human articular chondrocytes. Arthritis Rheum. 46:2368-2376.

Hung CC, Ichimura T, Stevens JL, and and Bonventre JV. 2003. Protection of renal cells against oxidative injury by endoplasmic reticulum stress preconditioning is mediated by ERK1/2 activation. J Biol Chem. 278:29317-29326.

Kaminska B. 2005. MAPK pathways as molecular targets for anti-inflammatory therapy-from molecular mechanisms to therapeutic benefits. Biochem Biophysica Acta.1754:253-262.

Keshavarzian A, Morgan G, Sedgu S, Gordon JH, and Doria M. 1990. Role of reactive oxygen metabolites in experimental colitis. Gut. 31:786-790.

Keshavarzian A, Haydek J, Zabihi R, Doria M, D'Astice M, and Sorenson JR.1992. Agents capable of eliminating reactive oxygen species, Catalase, WR-2721, or Cu(II)2(3,5-DIPS)4 decrease experimental colitis. Dig Dis Sci. 37:1866-1873.

Koon HW, Zhao D, Na X, Moyer MP, and Pothoulakis C. 2004. Metalloproteinases and transforming growth factor-alpha mediate substance P-induced mitogen-activated protein kinase activation and proliferation in human colonocytes. J Biol Chem. 279:45519-45527.

Mohler KM, Sleath PR, Fitzner JN, Cerretti DP, Alderson M, Kerwar SS, Torrance DS, Otten-Evans C, Greenstreet T, Weerawarna K, and Black RA. 1994. Protection against a lethal dose of endotoxin by an inhibitor of tumor necrosis factor processing. Nature. 370:218-220.

Na X, Zhao D, Koon HW, Kim H, Husmark J, Moyer MP, Pothoulakis C, and LaMont JT. 2005. Clostridium difficile toxin B activates the EGF receptor and ERK/MAP kinase pathway in human colonocytes. Gastroenterology. 128:1002-1011.

Nguyen DH, Catling AD, Webb DJ, Sankovic M, Wlker LA, Somlyo AV, Weber MJ, and Gonias SL. 1999. Myosin light chain kinase functions downstream of Ras/ERK to promote migration of urokinase-type plasminogen activator-stimulated cells in an integrin selective manner. J Cell Biol.146:149-164.

Podolsky DK. 2002. Inflammatory bowel disease**.** N Engl J Med. 347:417-429.

Prenzel N, Zwick E, Daub H, Leserer M, Abraham R, Wallasch C, and Ullrich A. 1999. EGF receptor transactivation by G-protein-coupled receptors requires metalloproteinase cleavage of proHB-EGF. Nature. 402:884-888.

Sanders SE, Madara JL, McGuirk DK, Gelman DS, and Colgan SP. 1995. Assessment of inflammatory events in epithelial permeability: a rapid screening

method using fluorescein dextrans. Epithelial Cell Biol. 4:25-34.

Santiskulvong C, and Rozengurt E. 2003. Galardin (GM6001), a broad-spectrum matrix metalloproteinase inhibitor, blocks bombesin- and LPA-induced EGF receptor transactivation and DNA synthesis in rat-1 cells. Exp Cell Res. 290:437-446.

Schafer B, Gschwind A, and Ullrich A. 2004. Multiple G-protein-coupled receptor signals converge on the epidermal growth factor receptor to promote migration and invasion. Oncogene. 23:991-999.

Scheving LA, Shiurba RA, Nguyen TD, and Gray GM. 1989. Epidermal growth factor receptor of the intestinal enterocytes. Localization to laterobasal but not brush border membrane. J Biol Chem. 264:1735-1741.

Schlondorff J, Becherer JD, and Blobel CP. 2000. Intracellular maturation and localization of the tumor necrosis factor alpha convertase. Biochem J. 347:131-138.

Singh AB, Tsukada T, Zent R, and Harris RC. 2004. Membrane associated HB-EGF modulates HGF-induced cellular responses in MDCK cells. J Cell Sci. 117:1365-1379.

Song J, Li J, Lulla A, Evers BM, and Chung DH. 2006. Protein kinase D protects against oxidative stress-induced intestinal epithelial cell injury via Rho/ROK/PKC-delta pathway activation. Am J Physiol Cell Physiol. 290:1469-1476.

Soond SM, Everson B, Riches DWH, and Murphy G. 2005. ERK-mediated phosphorylation of Thr735 in TNF-alpha converting enzyme and its potential role in TACE protein trafficking. J Cell Sci. 118:2371-2380.

Werb Z, and Yibing Y. 1998. A cellular striptease act. Science. 282:1279-1280.

Zeissig S, Bojarski C, Buergel N, Mankertz J, Zeitz M, Fromm M, Schulzke JD. Downregulation of epithelial apoptosis and barrier repair in active Crohn's disease by tumor necrosis factor-alpha antibody treatment. Gut 2004. 53:1295-1302.

Footnotes

This work was supported in part by a grant from Rush University Medical Center, Department of Internal Medicine, and by National Institutes of Health Grants NIDDK 60511 and NCCAM 01581 (to A.B.) and National Institute on Alcohol Abuse and Alcoholism Grant 13745 (to A.K.). Portions of this work were presented in the abstract form during the annual meeting of the American Gastroenterological Association (Digestive Disease Week), May 2006.

Address correspondence to:
Christopher B. Forsyth, PhD
Rush University Medical Center
Department of Internal Medicine, Section of Gastroenterology
1725 W. Harrison, Suite 206
Chicago, IL 60612
Email: christopher_b_forsyth@rush.edu

Legends for Figures

Figure 1. EGFR and TACE metalloprotease inhibitors prevent oxidant induced IEC permeability and changes in TJ protein ZO-1. *Fig. 1a. Permeability.* Confluent human intestinal epithelial cells (Caco-2) grown on inserts were assessed for permeability to FSA after 18h in serum-free (SF) media (see Methods). Permeability is expressed as FSA flux from apical to basal chamber (nmol/cm^2/h). Some cells were treated only with media or media + vehicle (DMSO) (hatched bars 1-5). Some cells were stimulated with oxidant (dark bars 6-10) at a dose determined by viability assay to have no effect on cell viability (0.5mM H_2O_2). In addition, some cells were pretreated (1h) with the EGFR-specific kinase inhibitor AG1478 (500 nM), the broad MMP-ADAM inhibitor GM6001 (20 μM), or the TACE-specific inhibitor TAPI-2 (10 μM). [Data are means ± S.D. of triplicate wells from a representative experiment from more than three separate experiments. Means compared by ANOVA were considered significant (*, p≤ 0.05), for bars 2-5 compared to bar1, and for bars 7-10 compared to H_2O_2 control bar 6. *Fig. 1b. ZO-1 staining.* Confluent Caco-2 IEC grown on glass coverslips were washed with PBS and treated for 30 min with SF media + DMSO vehicle or media + H_2O_2 (0.5 mM). In addition, some cells were pretreated (1h) with the EGFR-specific kinase inhibitor AG1478 (500 nM) or the TACE-specific inhibitor TAPI-2 (10uM) before oxidant treatment. Cells were then washed, permeabilized, and stained with Ab to ZO-1 and FITC anti-mouse secondary Ab. Images (100x) are representative of more than 100 images taken for each condition in more than three experiments. Figure 1c. Effect of ERK1/2

inhibitor on oxidant-induced barrier hyperpermeability and cell signaling. Confluent Caco-2 monolayers on inserts were assessed for oxidant-induced permeability in the absence or presence of inhibitor to ERK1/2 (PD98059, 20uM) as in Fig. 1a. (media alone hatched bar; bar 2 H_2O_2 0.5 mM:, bar 3 H_2O_2 + PD98059). Cells were pre-incubated with inhibitor 1h. Data are means of triplicate wells from a representative of more than three experiments. Figure 1d. Effect of EGFR, TACE, and ERK1/2 inhibition on permeability to 4kd FITC-dextran. Confluent Caco-2 monolayers on inserts were assessed for permeability to 4kd FITC-labeled dextran under the same conditions described in 1a. (vehicle is 1.0% DMSO, EGFRi= AG1478 500nM; MMPi= TAPI-2 10uM; ERKi= PD98059 20uM). Data are means ± SD of triplicate wells from one of three experiments.

Figure 2. Phosphoprotein analysis of H_2O_2-induced EGFR and ERK1/2 phosphorylation. Fig. 2a. Phosphorylation of EGFR. Cells grown on culture inserts were treated for 10 min and cell lysates were assessed for EGFR phosphorylation by WB with Ab specific for EGFR phosphotyrosine # 1068 and stripped and reprobed with Ab to total EGFR to control for protein loading (lower). Cells in lanes 3-10 were treated with H_2O_2 (0.5 mM) ± the same inhibitors and concentrations as in Fig. 1a and 1b. Image shown is from a representative experiment from more than three experiments and all images in Fig. 2 a/b and Fig. 3 are from the same representative experiment lysates. Blots were developed with ECL and film and scanned. Three separate blot scans were analyzed using Image J software (NIH) and the densitometry shown as means of uncalibrated O.D. ± S.D. as a percent of the H_2O_2 positive control (100%). Fig.

2b. ERK1/2 phosphorylation. Cell lysates described in Fig. 2a were also assessed separately by Western blot using Ab to phospho-ERK1/2. Lanes were equalized for total protein (20ug) and also stripped and reprobed for total ERK/12 to control for loading. Positive phospho-ERK1/2 control in lane 1: "+Con" (Cell Signaling). Densitometry results for three blot scan means ± SD are shown below.

Figure 3. EGFR and TACE inhibitors also block H_2O_2-induced ERK1/2 activation in IEC-6 cells. IEC-6 (rat, non-transformed) intestinal epithelial cells were also assessed for EGFR-metalloprotease signaling in response to stimulation with H_2O_2. Confluent cells grown on inserts were treated as in Fig. 2 above.

Figure 4. SiRNA knockdown of TACE blocks H_2O_2-stimulated ERK1/2 activation. Caco-2 cells grown to 60% confluency were transfected with Dharmacon Smartpool siRNA (60pM) to TACE (human ADAM-17) as described in Methods, allowed to rest for 24h and transfected with another round of Dharmacon Smartpool siRNA (60pM) to TACE. After 7 days, for ERK1/2 activation assessment cells were treated as in Fig. 2 above and cell lysates were evaluated by Western blot for ERK1/2 phosphorylation and total ERK1/2. Blots were stripped and reprobed for TACE 110 kd precursor and TACE 90 kd activated protein expression (upper panel). Densitometry with Image J revealed 84% knockdown of TACE protein and 85% reduction of ERK1/2 activation compared to cells treated with control scrambled RNA (Dharmacon).

Figure 5. Western blotting of TACE protein expression. Cell lysates from the same representative signaling experiment used for Fig. 2a and 2b were

assessed for TACE expression using Ab to the TACE cytoplasmic domain which identifies the precursor (110 kd) and the active enzyme (90 kd). A TACE positive control lysate (+Con) (Chemicon) is in lane 1. The blot was stripped and reprobed for actin as a control for protein loading (lower panel).

Figure. 6. Real time quantitative RT-PCR analysis of Caco-2 cell TACE expression. RNA was isolated from Caco-2 cells treated under the conditions shown for zero or 18h 'overnight': H_2O_2: 0.5 mM; H_2O_2 + EGFR inhibitor AG1478 500 nM; H_2O_2 + EGF 10ng/ml. Then RNA from each sample was subjected to quantitative RT-PCR for TACE expression as well as beta-actin expression as internal control (Methods) and data were normalized for expression relative first to beta-actin and then to control start expression (vehicle treated=1.0). Data are from triplicate wells from one of three experiments and expressed as means ± SD.

Figure 7. Blocking Abs to EGFR and TGF-α block oxidant-induced increase in permeability in IEC monolayers. Caco-2 cells grown on inserts as described in Fig. 1 were either not treated (hatched) or treated (solid) with 0.5mM H_2O_2 and assessed for permeability to FSA. Some cells were pretreated with the following inhibitors: Bars 2 and 6: blocking Ab to the EGFR extracellular domain (LA1, 500nM); Bars 3 and 7 : blocking protein to HB-EGF (CRM197 500 nM); Bars 4 and 8: blocking Ab to TGF-α (R&D, 500M). Data are means ± SD of triplicate values from a representative of three experiments.

Figure 8. Blocking Abs to the EGFR and TGF-α inhibit oxidant-induced EGFR phosphorylation. Confluent Caco-2 cells were treated with media (control) or for 10 min with oxidant (H_2O_2, 0.5 mM) ± the following: EGFRi: AG1478 500 nM; TACEi: TAPI-2 10 μM; EGFR Ab: LA1 blocking Ab 500 nM; TGF-α Ab: R&D blocking Ab 500 nM; HB-EGFi: CRM197 500 nM. Cells were pre-incubated with inhibitors for 1 h. Cell lysates equalized for total protein were analyzed by Western blot (Methods). The blot shown is a representative of three experiments. Phosphotyrosine Ab 4E10 (upper panel with phospho-EGFR control). Data shown are means ± SD of three blot scans assessed using Image J densitometry software. Treatment with Ab to amphiregulin (500nM) had no inhibitory effect (not shown).

Figure 9. Blocking Abs to TGF–α eliminate oxidant-induced ERK1/2 activation. Cell lysates from the identical representative experiment as detailed in Fig. 8 were also assessed for ERK1/2 phosphorylation, stripped and reprobed for total ERK1/2, and assessed by densitometry using Image J software. Data are means ± SD of three blot scans from a representative of more than 3 experiments.

Figure 10. The EGFR is localized to cell-cell contact zones. Confluent monolayers of Caco-2 cells grown on glass coverslips were treated with blocking Ab to the EGFR extracellular domain + FITC 2°Ab (green) and Ab to TACE + Texas Red 2°Ab (red). White arrows shows EGFR localization to cell-cell contact zones (100x).

Figure 11. The EGFR surface proligands HB-EGF and TGF-α are also localized to cell-cell contact zones. Caco-2 cells grown on glass coverslips were treated with primary Ab to either HB-EGF (9a) or TGF-α (9b) followed by FITC secondary Ab. White arrows denote staining concentrated in cell-cell contact zones (100x).

Figure 12. Oxidant stimulates TACE movement to cell-cell junction zones. Caco-2 cells cultured on glass coverslips as in Figs. 8 and 9 were treated with media alone (upper panels, a-c) or oxidant (H_2O_2, 0.5 mM)(lower panels, d-f) for 30 min. Cells were washed, fixed/permeabilized and treated with Ab to ZO-1 and TACE. After washing, cells were treated with anti-mouse FITC (ZO-1) or anti-rabbit Texas Red (TACE). White arrows indicate TACE staining in the two sets of panels. Note the distinct ring-like movement of TACE to cell-cell contact zones in the H_2O_2-stimulated (lower) images (100x).

Figure 13. X-Z and X-Y views of TACE and ZO-1 reveals movement of TACE in H_2O_2-stimulated cells to co-localize with ZO-1. Caco-2 cells grown on glass coverslips and treated as in Fig. 12 including identical primary and secondary Ab treatment: TACE: Texas Red; ZO-1: FITC (green). Then, 15 z-stack images (each 1μm) were taken using an oil immersion 40x objective and deconvoluted and combined using computer software (Zeiss Axiovision). White arrow shows TACE predominately distributed below the plane of ZO-1 (tight junctions) in

unstimulated cells (Fig. 13a) while clearly moving to the pane of ZO-1 in the H_2O_2-stimulated cells (Fig. 13b)(40x oil immersion).

Figure 14. 3-Dimensional reconstruction of deconvoluted z-stack data from Fig. 13 also shows TACE segregated from ZO-1 in unstimulated cells with TACE-ZO-1 colocalization in H_2O_2-stimulated cells. The pictures shown in this figure were constructed from the identical deconvoluted z-stack data used to make the images in Fig. 13 (40x oil immersion).

Figure 15. Proposed model for TACE metalloprotease-mediated EGFR regulation of intestinal permeability in response to oxidant stress. The model depicts the major elements we propose in a new mechanism for intestinal hyperpermeability induced by oxidant stress. This model is based on our own novel data (steps 3-6) and previous work by others. Proposed steps are numbered in order of occurrence. **1)** The process begins with H_2O_2 (oxidant stress) initiating cell signals through activation of TACE . **2)** TACE activation. **3)** TACE activation results in translocation to cell-cell contact zones where it cleaves TGF-α proligand to form soluble TGF-α that then binds to the EGFR. **4)** EGFR becomes phosphorylated and activates downstream MAPK signals including ERK1/2. **5)** Activated ERK1/2 then phosphorylate cellular targets (MLCK? Occludin?) **6)** These ERK1/2 targets then mediate changes in intestinal permeability.

Figure 1.

1a.

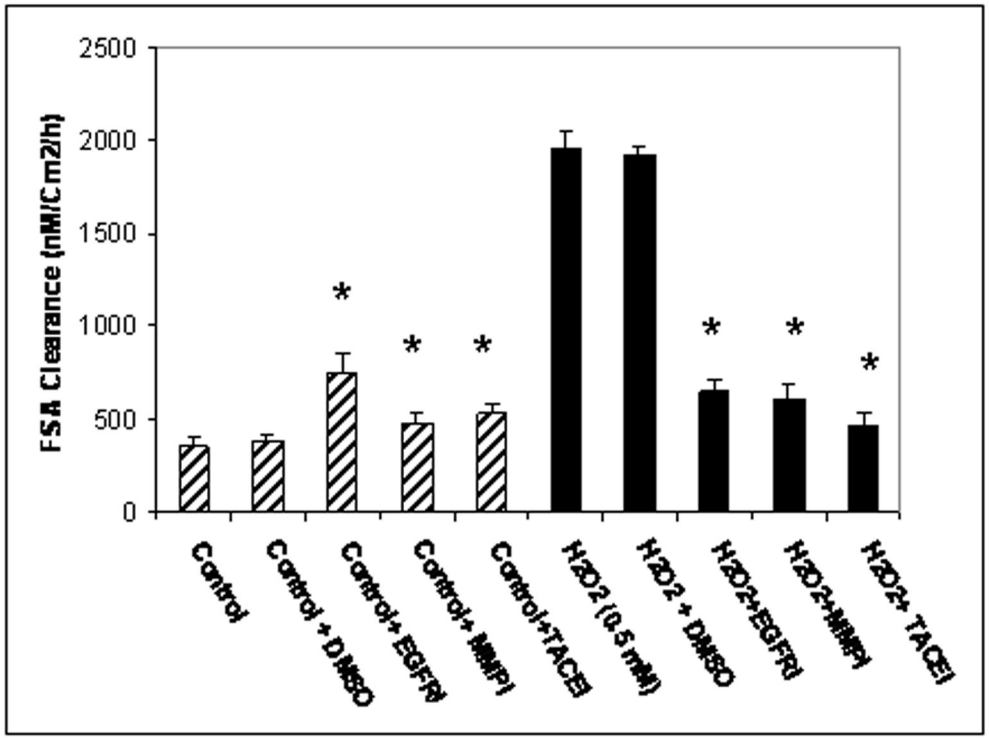

1b.

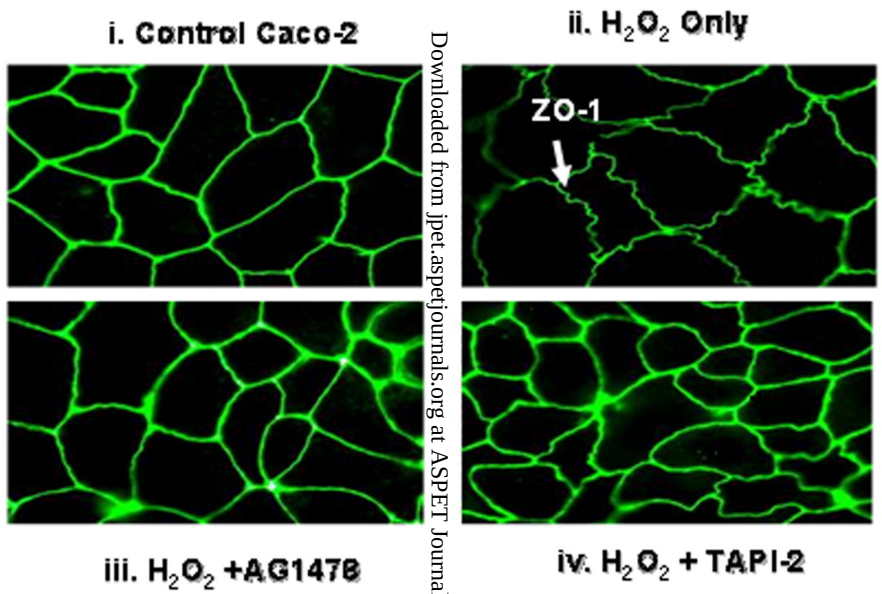

1c.

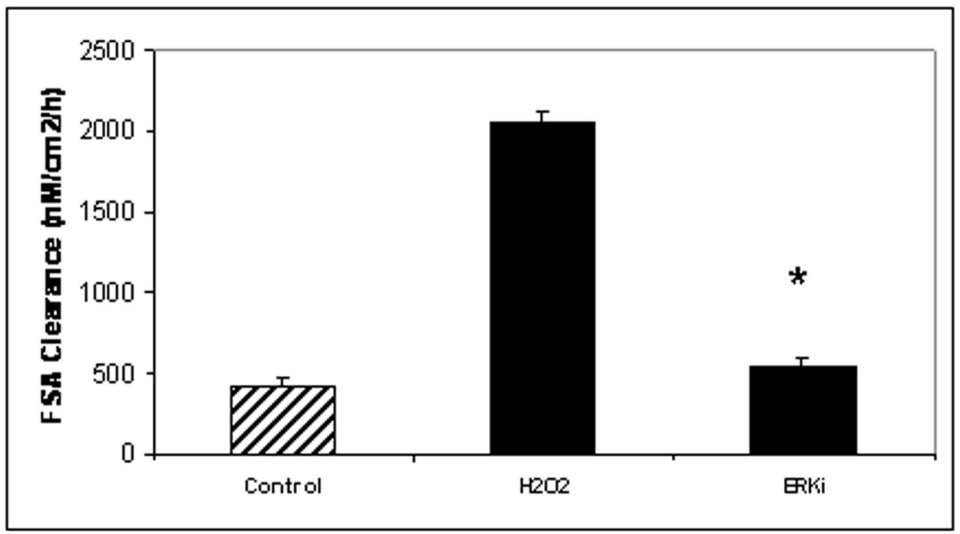

1d.

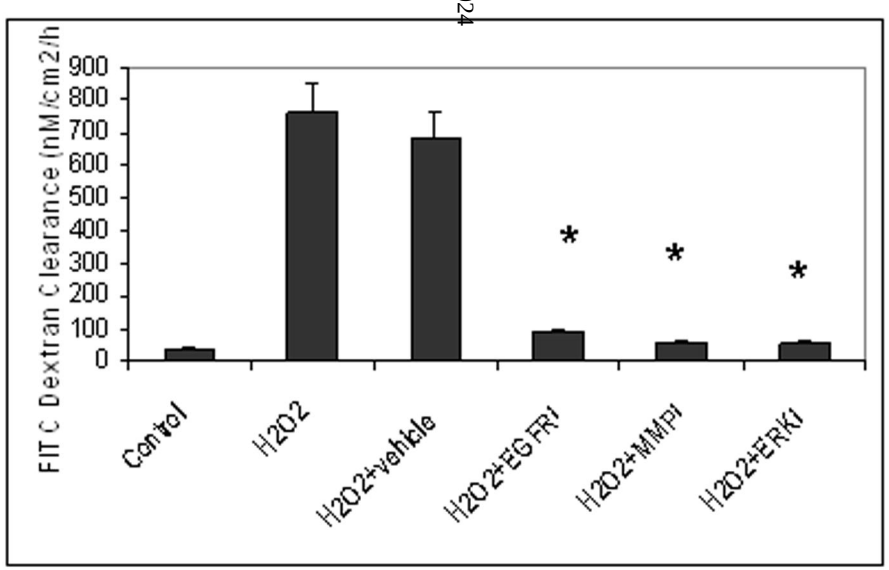

Figure 2.

2a.

	Con	H_2O_2	EGFRi	TACEi	ERKi
H_2O_2:	-	+	+	+	+
Lanes:	1	2	3	4	5

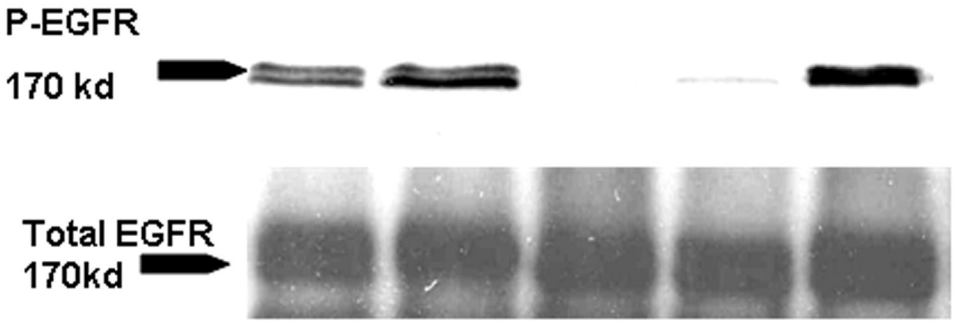

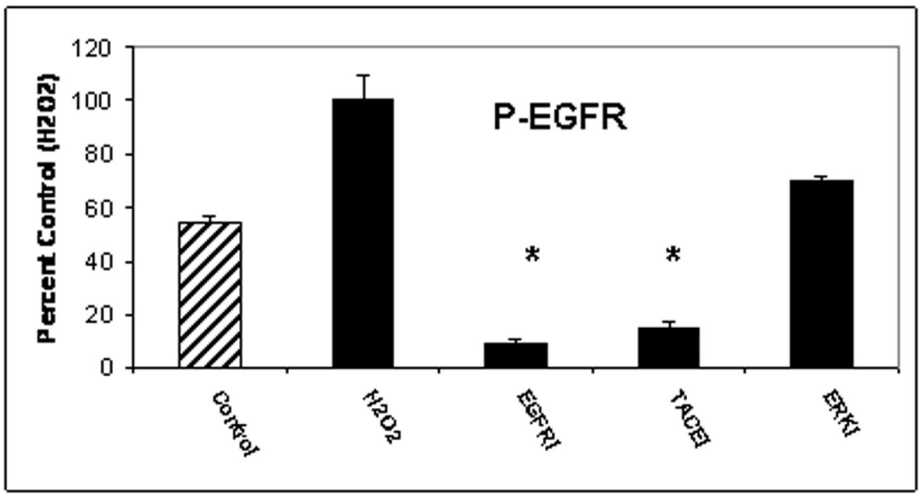

2b.

	+Con	Con	H_2O_2	EGFRi	TACEi	ERKi
H_2O_2	-	-	+	+	+	+
Lane	1	2	3	4	5	6

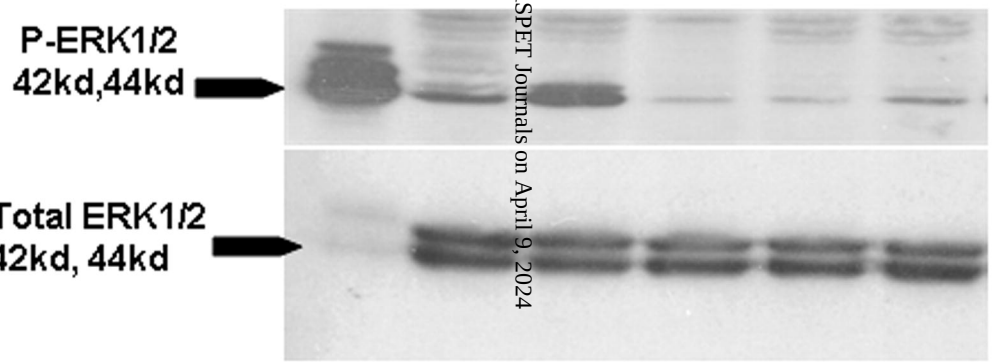

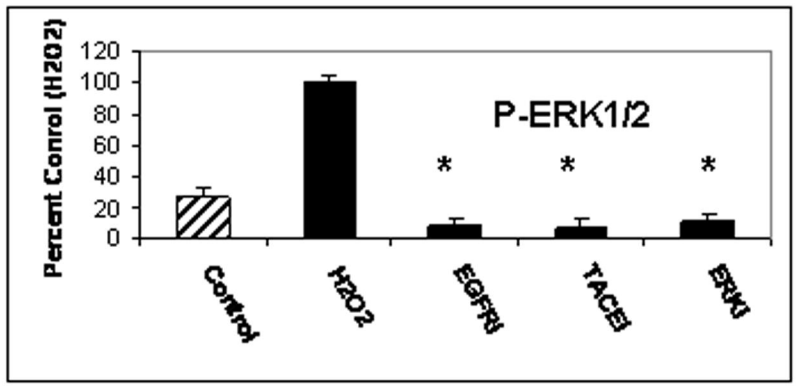

Figure 3.

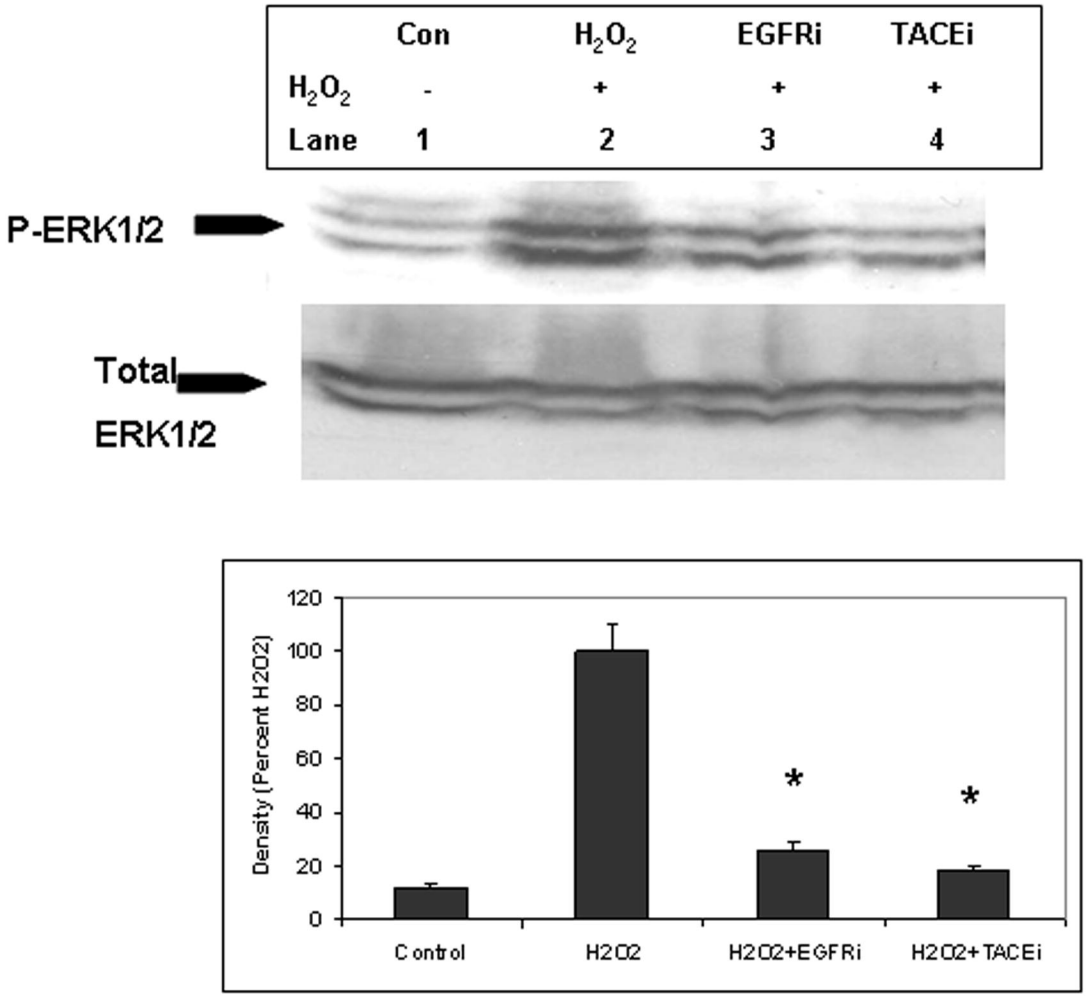

Figure 4.

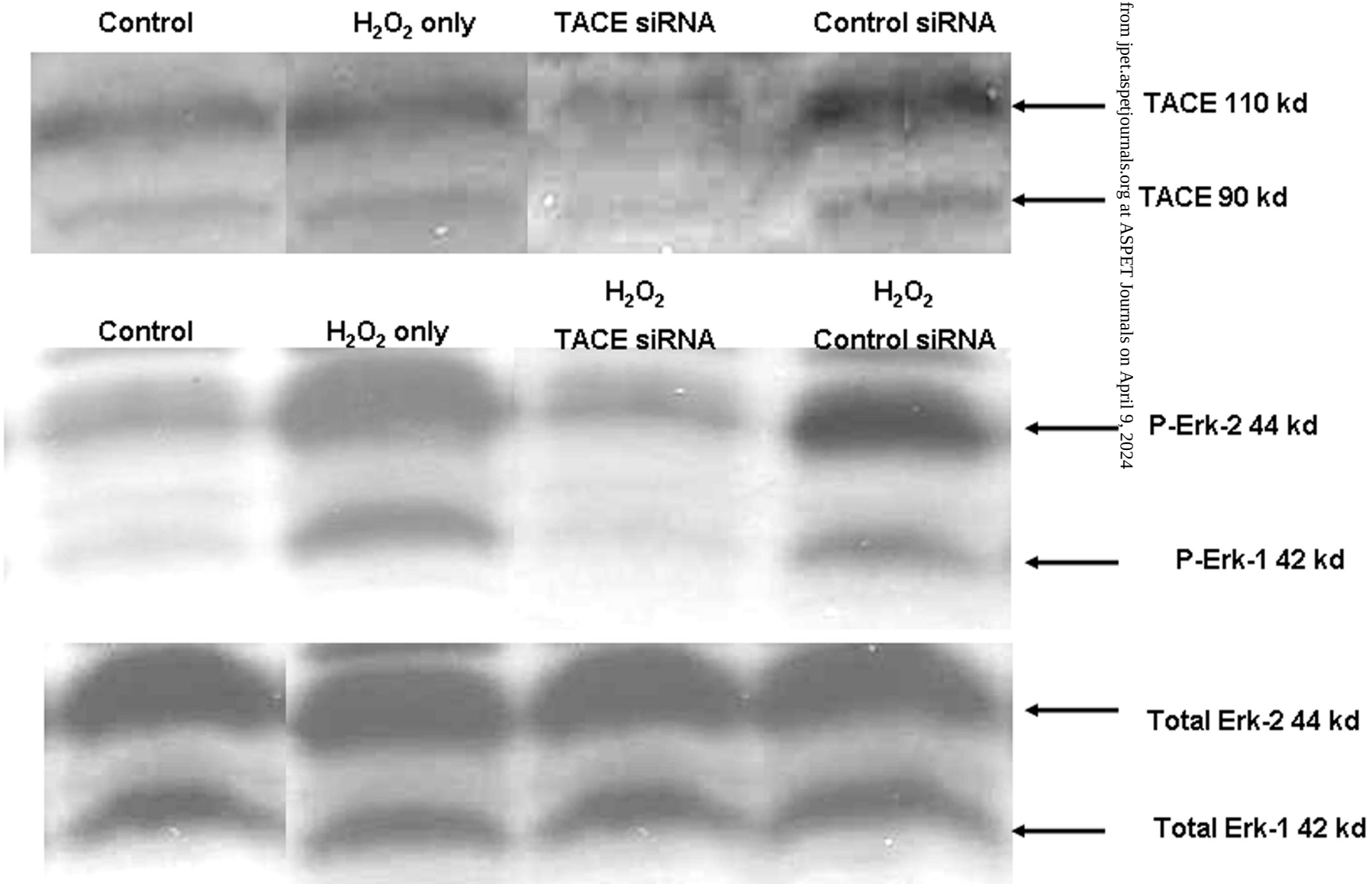

Figure 5.

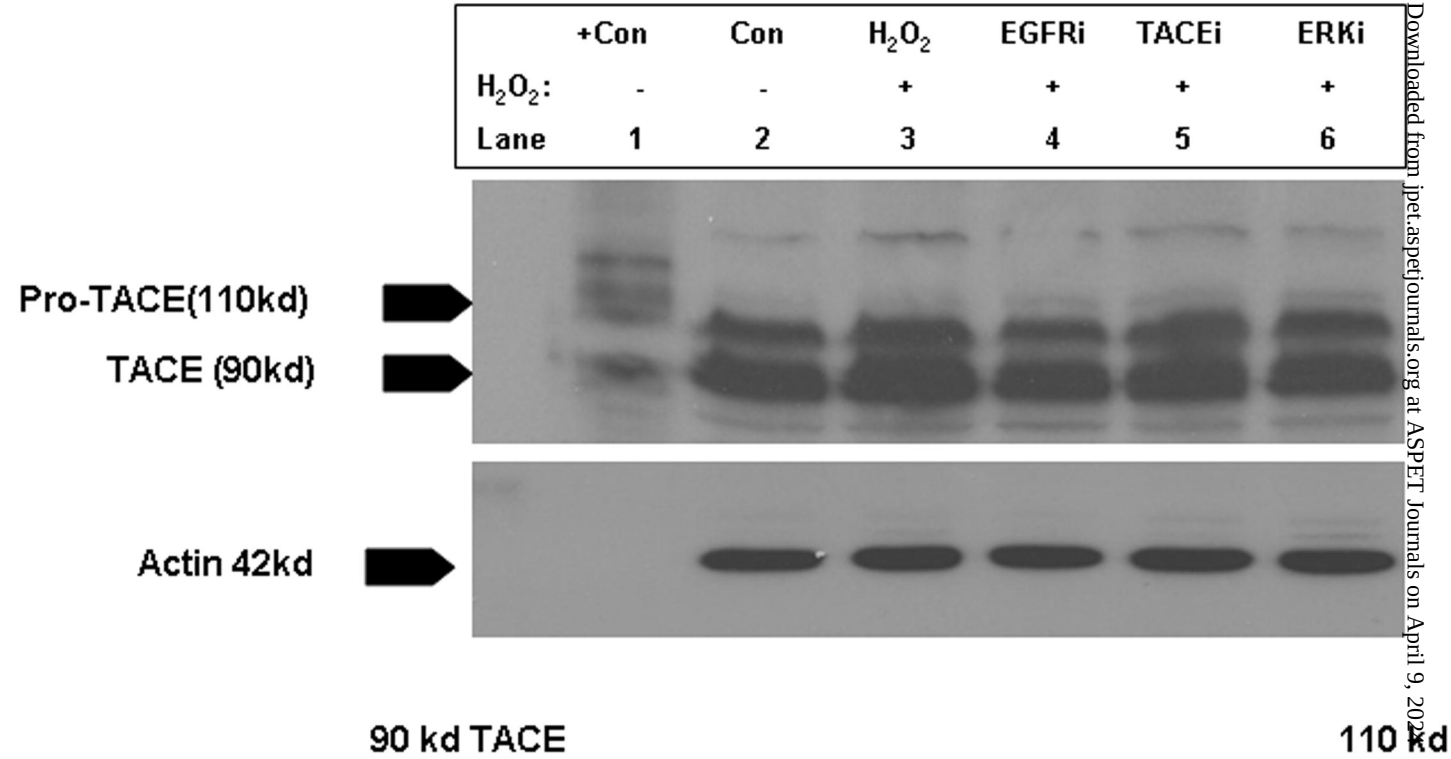

90 kd TACE

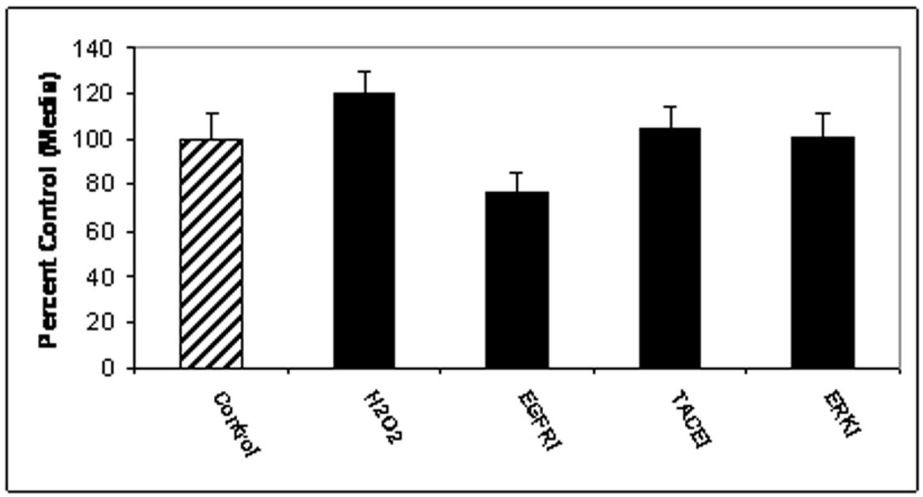

110 kd TACE

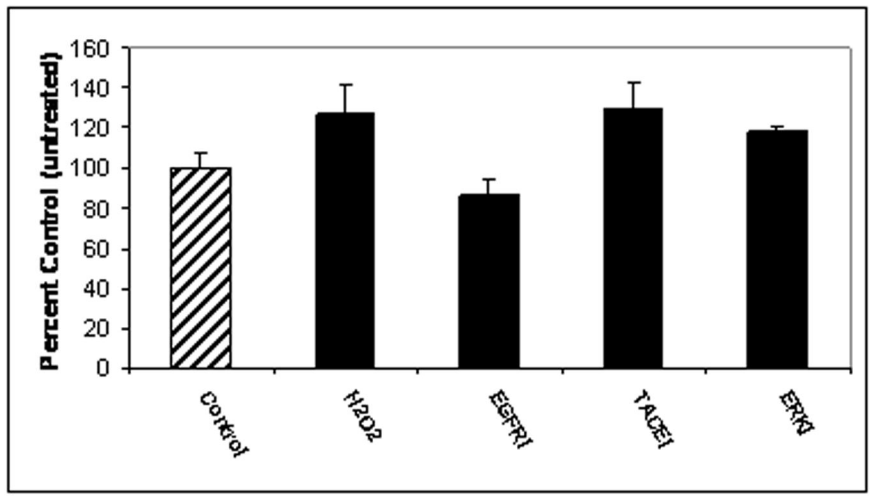

Figure 6.

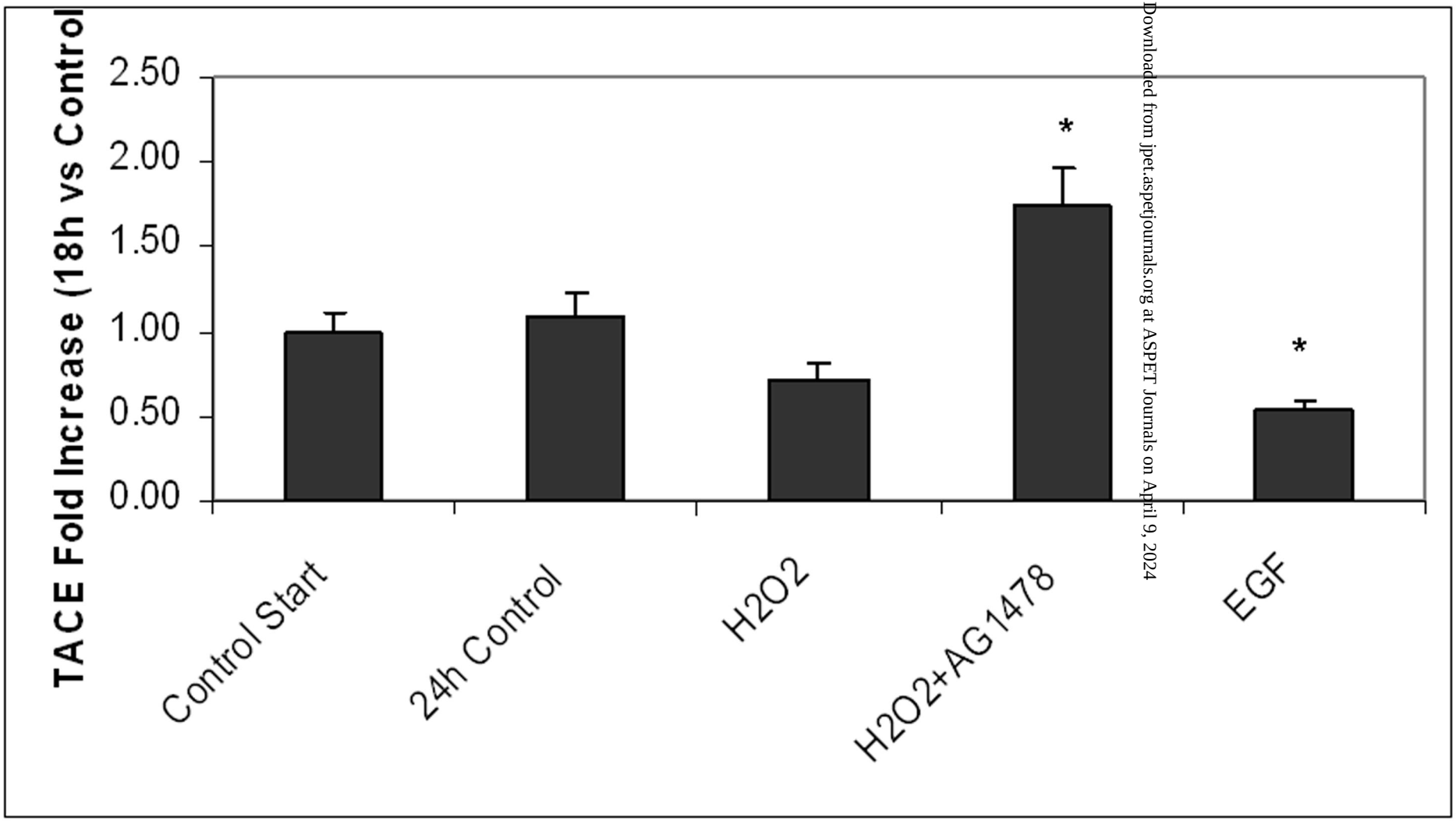

Figure 7.

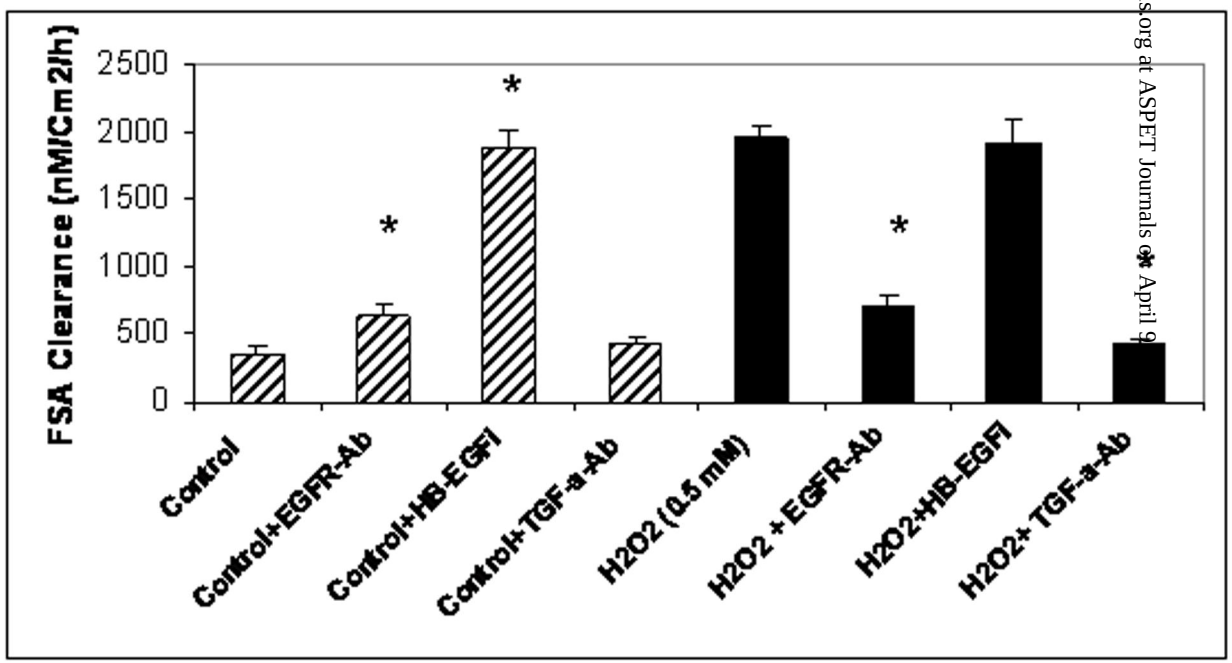

Figure 8.

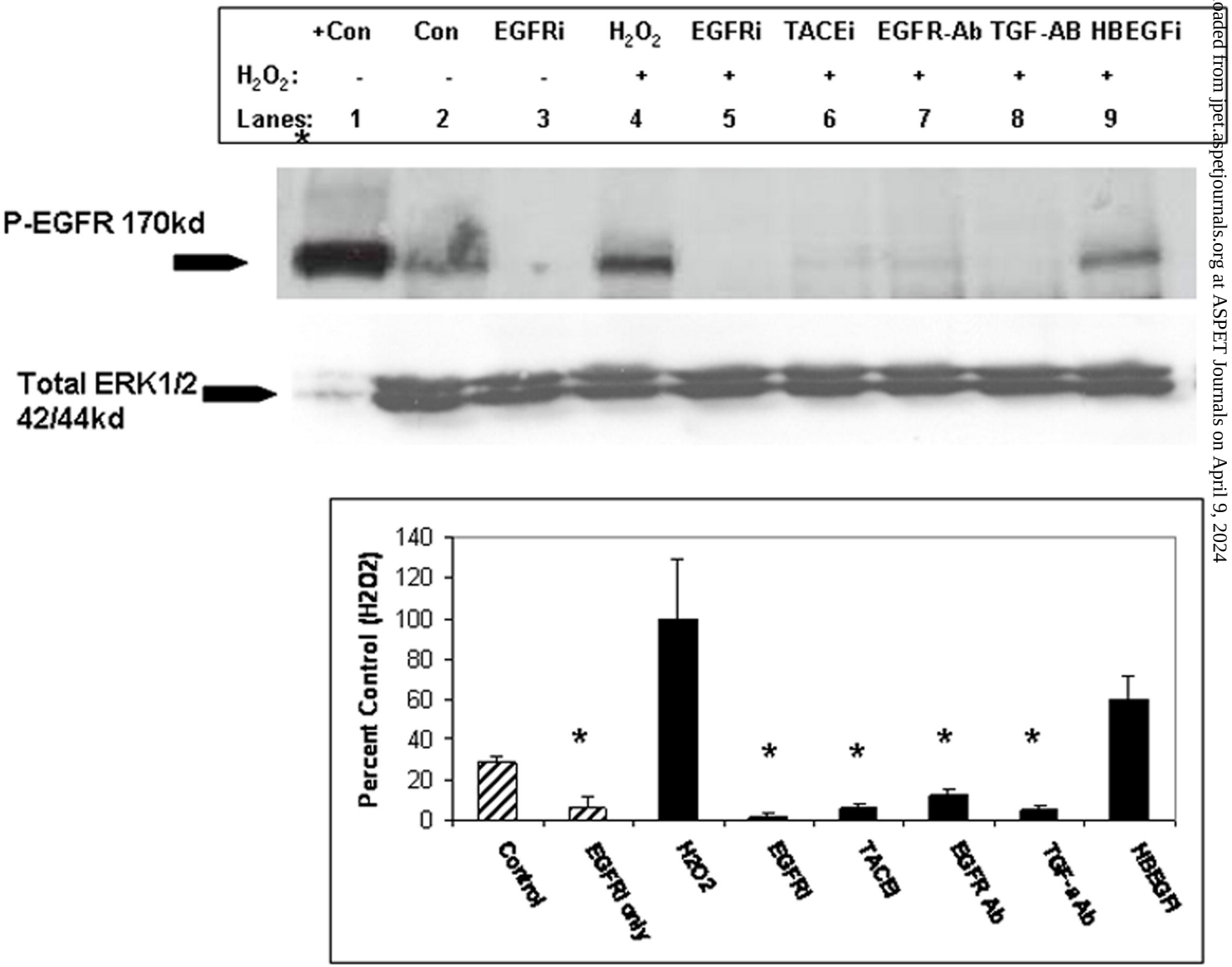

Figure 9.

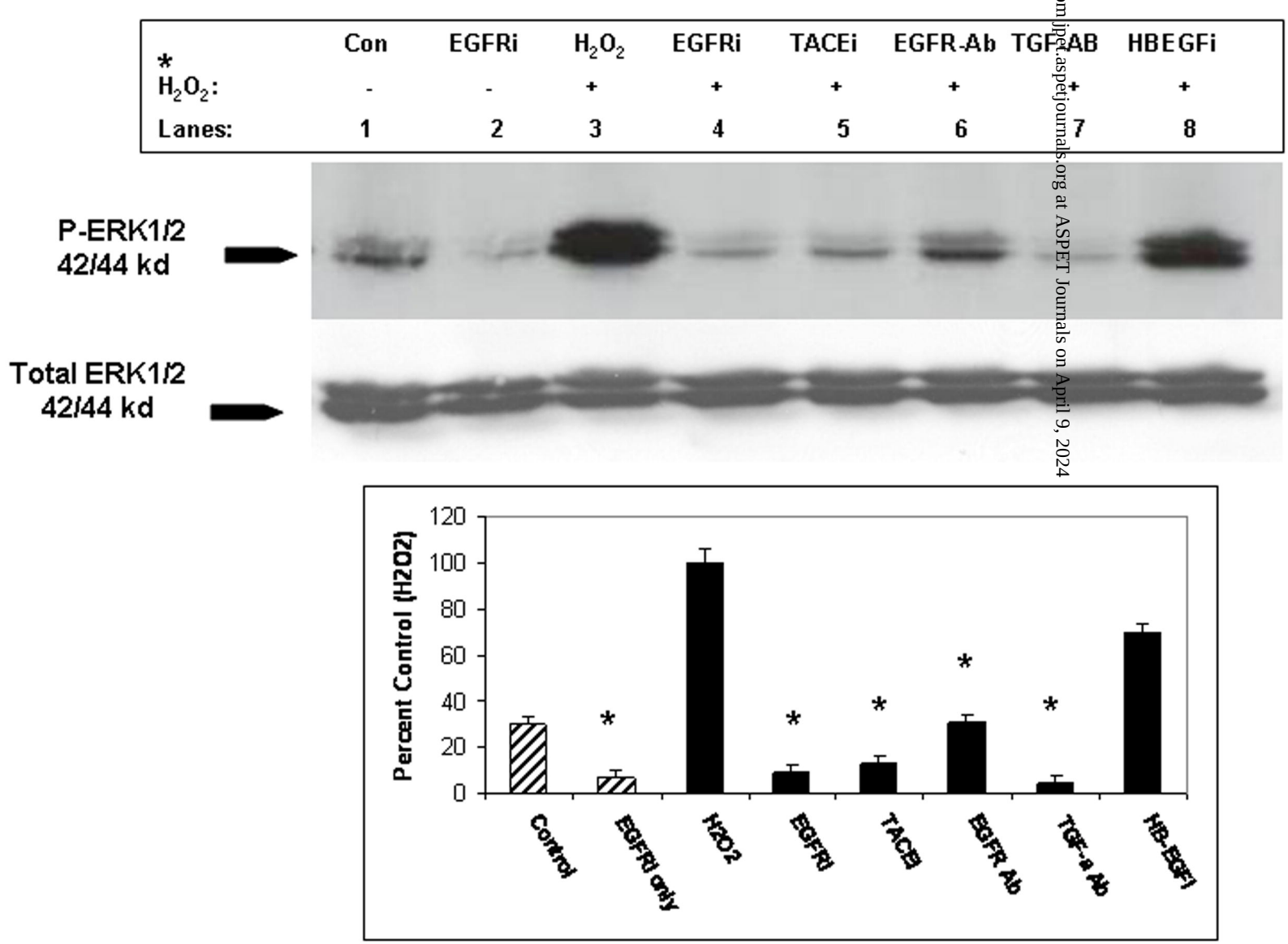

Figure 10.

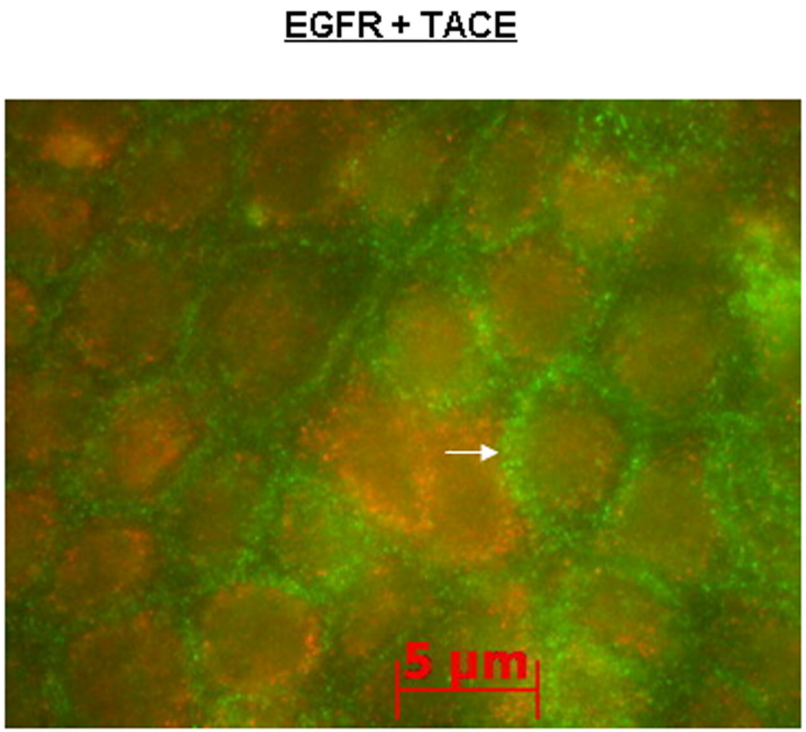

FIGURE 11.

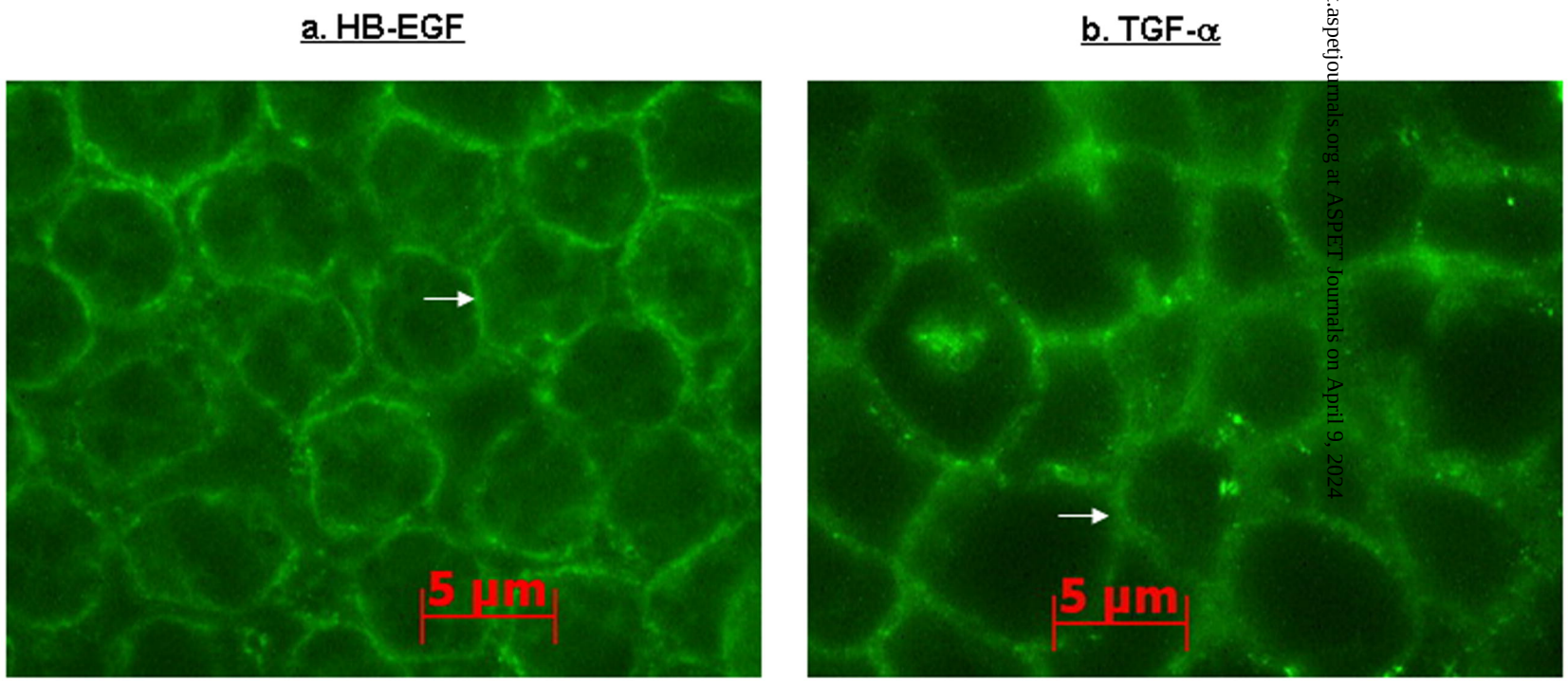

FIGURE 12.

CONTROL UNTREATED

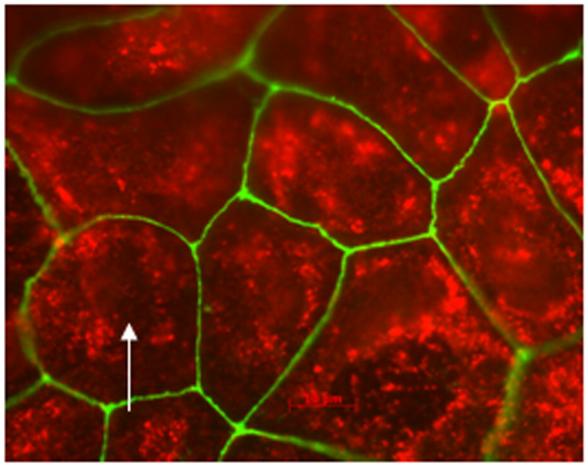

a. TACE + ZO-1

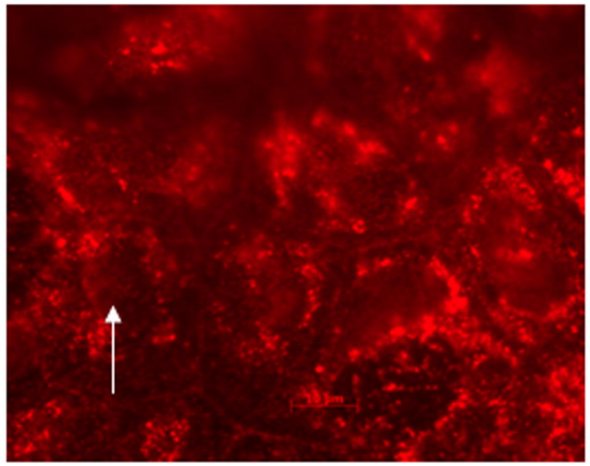

b. TACE

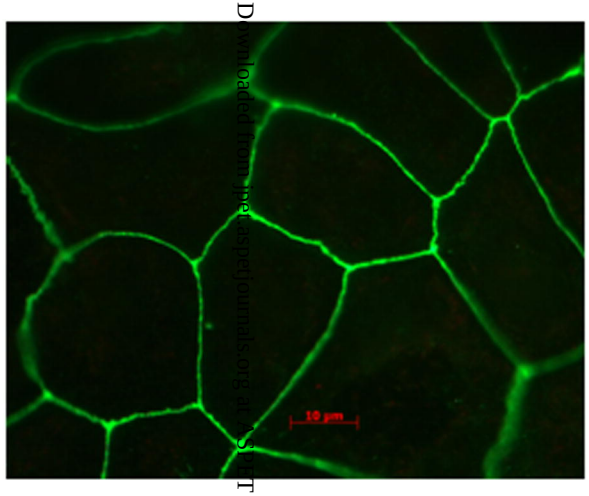

c. ZO-1

H_2O_2 STIMULATED

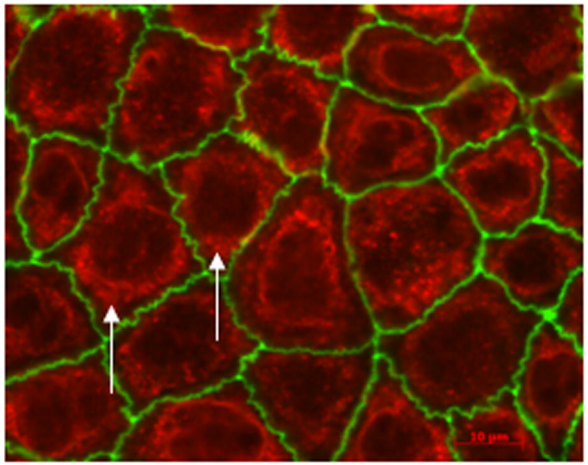

d. TACE + ZO-1

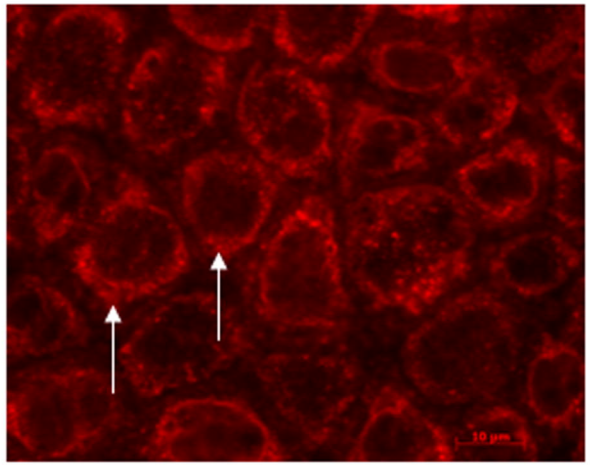

e. TACE

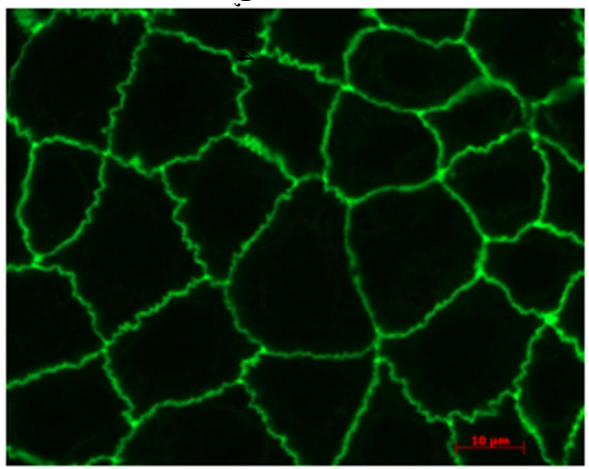

f. ZO-1

FIGURE 13.

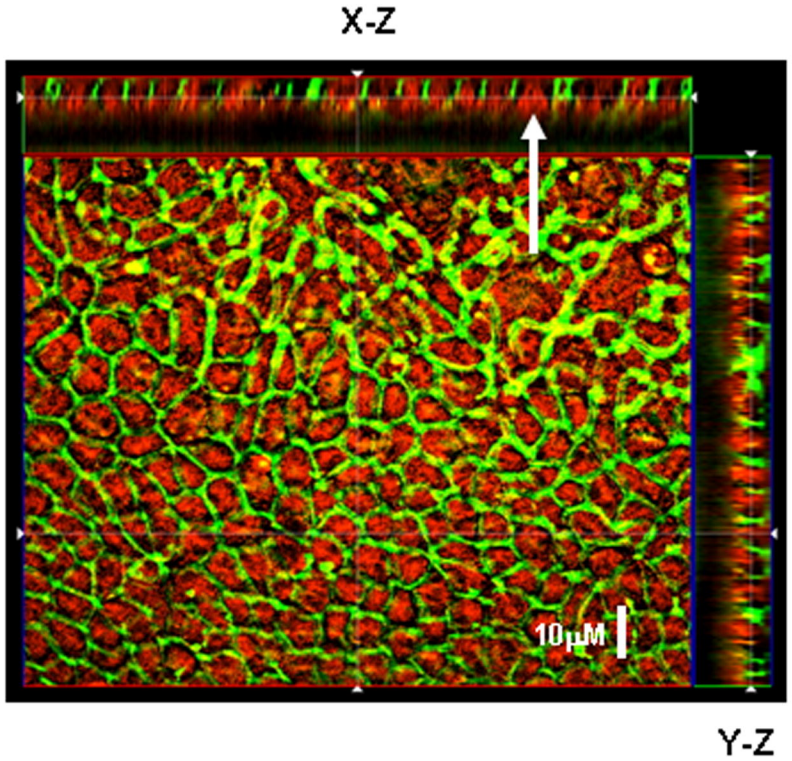

13a. CONTROL

(ZO-1+TACE)

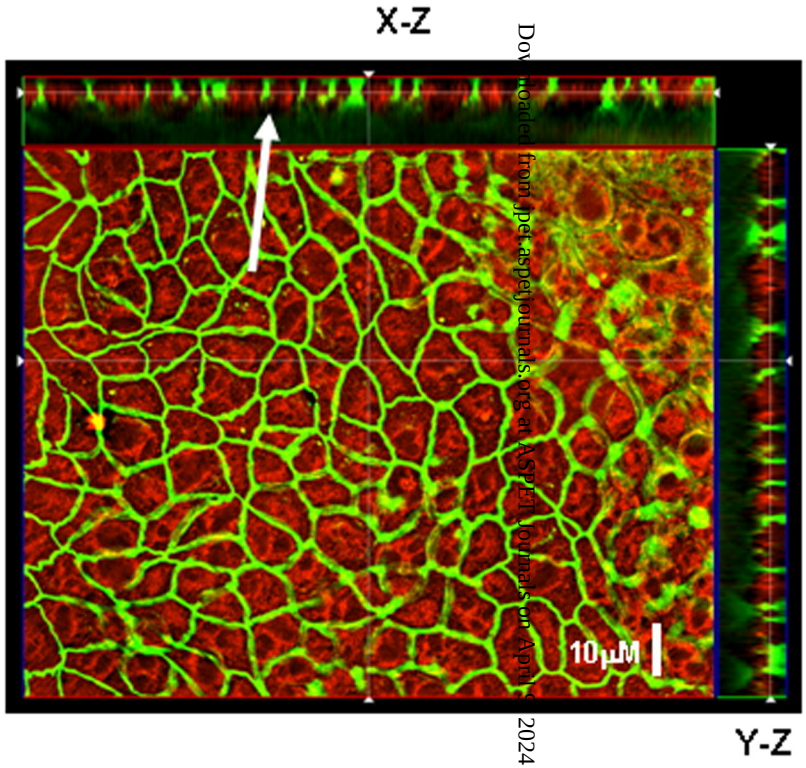

13b. H_2O_2-TREATED

(ZO-1+TACE)

FIGURE 14.

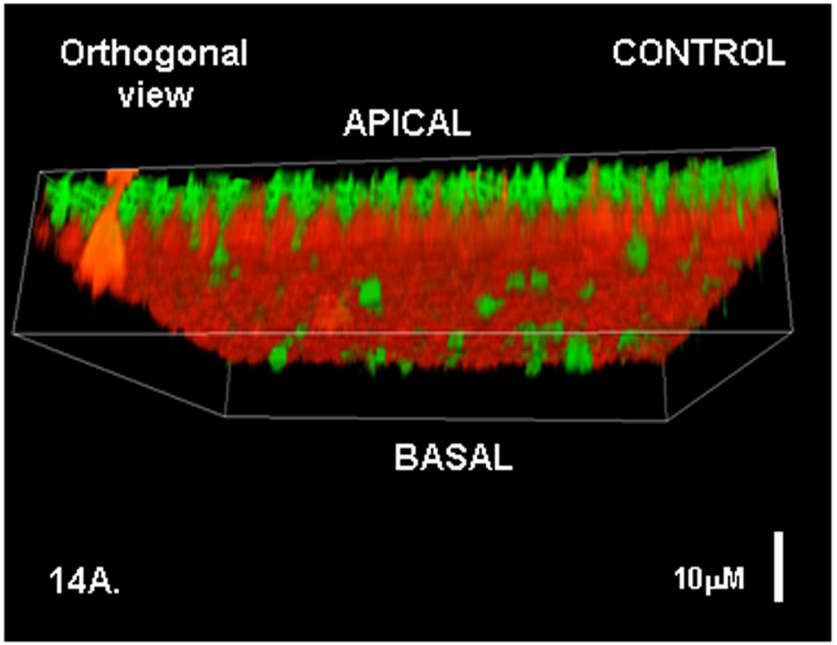

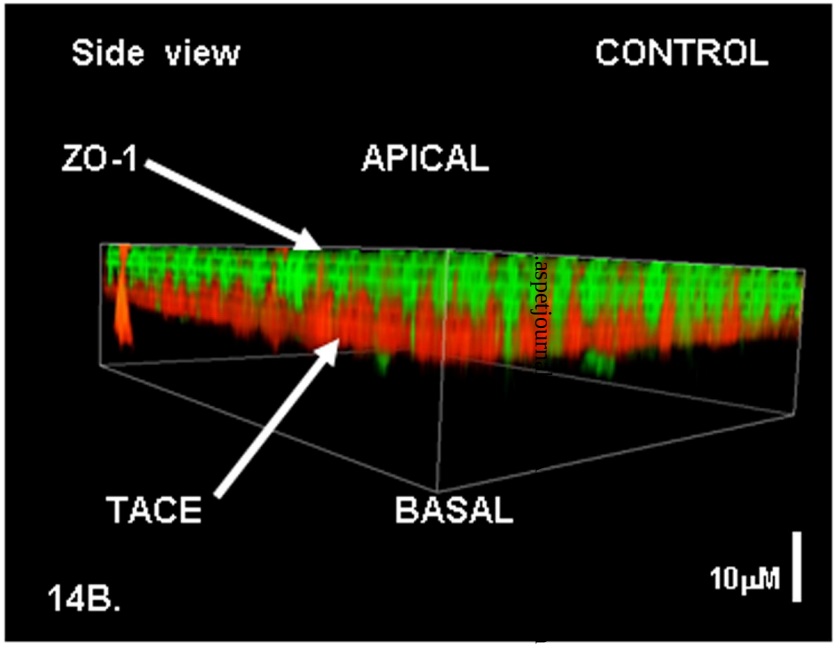

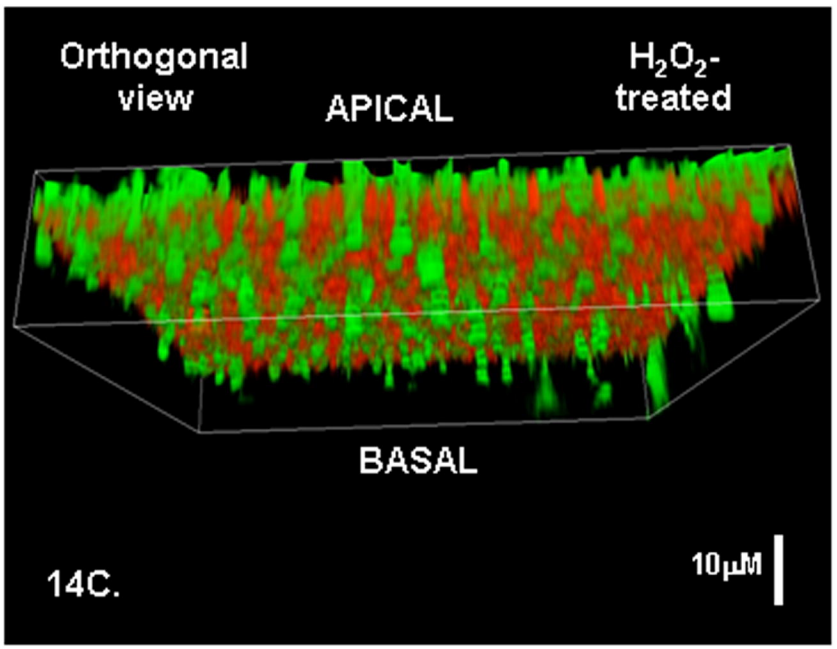

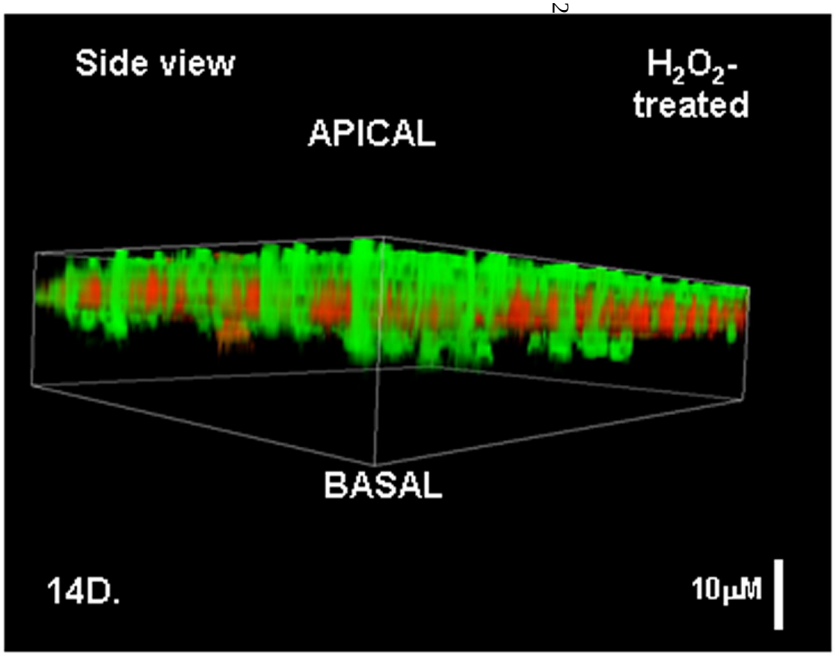

Figure 15.